OPEN

ORIGINAL ARTICLE

Regulation of spindle integrity and mitotic fidelity by BCCIP

SC Huhn[1,2], J Liu[1,2], C Ye[1,2], H Lu[1,2], X Jiang[1,2,5], X Feng[1,2], S Ganesan[1,3], E White[1,4] and Z Shen[1,2]

Centrosomes together with the mitotic spindle ensure the faithful distribution of chromosomes between daughter cells, and spindle orientation is a major determinant of cell fate during tissue regeneration. Spindle defects are not only an impetus of chromosome instability but are also a cause of developmental disorders involving defective asymmetric cell division. In this work, we demonstrate BCCIP, especially BCCIPα, as a previously unidentified component of the mitotic spindle pole and the centrosome. We demonstrate that BCCIP localizes proximal to the mother centriole and participates in microtubule organization and then redistributes to the spindle pole to ensure faithful spindle architecture. We find that BCCIP depletion leads to morphological defects, disoriented mitotic spindles, chromosome congression defects and delayed mitotic progression. Our study identifies BCCIP as a novel factor critical for microtubule regulation and explicates a mechanism utilized by BCCIP in tumor suppression.

INTRODUCTION

During mitosis, both the faultless segregation of newly duplicated chromosomes and the proper positioning of daughter cells require an elegant mitotic apparatus, a complex microtubule-based protein machine organized in a bipolar fashion.[1] The assembly of the mitotic apparatus occurs *de novo* once, and only once, per cell cycle and requires a high level of cooperation between microtubules, centrosomes, microtubule-associated proteins (MAPs) and molecular motors.[1,2] Factors that compromise the reliability of the mitotic apparatus cause aneuploidy, a hallmark of cancer and the rate-limiting step in tumorigenic transformation.[2–6] Faithful spindle assembly is critical not only for chromosome distribution but also for the three-dimensional orientation of the spindle.[3,7] Mitotic spindle orientation is regulated by the interplay between centrosomes, microtubules and molecular motors, and it is critical for stem cell polarity and tissue regeneration.[8,9] This pathway also plays a pivotal role in cell division-directed differentiation.[8,9] In addition, a link between the fidelity of spindle orientation and tumor formation has been recognized in the context of cancer stem cell renewal.[10] Thus, the characterization of factors, which destabilize the mitotic apparatus, is not only of importance to understand the nature of aneuploid diseases, such as cancer, but also for stem cell renewal, tissue development and regeneration.

The principal microtubule organizing center of the cell is known as the centrosome. It consists of an orthogonal pair of centrioles enveloped by a mesh of an electron-dense material known as the pericentriolar matrix.[11–13]

One centriole, known as the mother centriole, is one full cell cycle older than its counterpart and contains unique protein complexes responsible for organizing the cell's microtubule network into a single point-like focus.[11] This function, known as microtubule anchoring, is strictly associated with the mother centriole and is paramount for directing cell polarity, shape and motility as well as orienting the cell axis during division.[8–11,14] During mitosis, centrosomes play an integral role in chromosome capture by nucleating soluble tubulin subunits into the polymeric microtubules that comprise the spindle. Following microtubule nucleation, centrosomes are focused by a series of motor proteins into two distinct spindle poles containing a meshwork of microtubule regulators. The focusing of each centrosome into a distinct spindle pole matrix is thought to increase spindle tension and chromosome segregation fidelity by transducing negative-end motor force.[1,15,16] Among these constituents, the minus-end directed motor dynein, is vital for pole establishment.[1,15] Dynein activities are regulated through its processivity factor, dynactin, a component also found in the mother centriole that regulates the centrosome's microtubule anchoring and stabilizing capabilities.[17–20] Dynein/dynactin also cooperate with minus-end MAPs, such as NuMa, which sequester, stabilize and bundle microtubules at the poles.[8,16,21] Thus, the interplay between centrosomes, molecular motors and MAPs is intimately linked to ensure faithfulness of mitosis.

BCCIP was initially identified as a BRCA2 and p21 interacting protein and is essential for cell viability in mice and budding yeast.[22–27] Despite a high degree of evolutionary conservation across all eukaryotes, the structure and function of the BCCIP gene is not fully understood. Canonically, BCCIP is thought to regulate DNA damage response, suppress spontaneous DNA damage and modulate the G1/S transition through the cell cycle.[23–26,28] Concurrently, this view of BCCIP has also been expanded to include roles in cytoskeletal rearrangement, ribosome biogenesis and nuclear export.[22–27,29–31] In *Homo sapiens*, two major BCCIP isoforms that result from alternative splicing exist, designated as BCCIPα (322 amino acids) and BCCIPβ (314aa).[32] These two isoforms share an identical conserved domain spanning ~ 258aa but are diversified by unique C termini.[32] Thus, it is likely that in humans BCCIPα and BCCIPβ have evolved to further specify the function of the sole BCCIP gene present in other eukaryotes. BCCIP loss has been implicated in numerical chromosome instability and polyploidization, and partial and non-permanent loss of BCCIP can spur tumorigenesis in mice.[26,29]

[1]Rutgers Cancer Institute of New Jersey, 195 Little Albany Street, New Brunswick, New Jersey 08903, USA; [2]Department of Radiation Oncology, Rutgers Robert Wood Johnson Medical School, New Brunswick, New Jersey, USA; [3]Department of Medicine, Rutgers Robert Wood Johnson Medical School, New Brunswick, New Jersey, USA and [4]Department of Molecular Biology and Biochemistry, Rutgers, The State University of New Jersey, Piscataway, New Jersey, USA. Correspondence: Professor Z Shen, Department of Radiation Oncology, Rutgers Cancer Institute of New Jersey/Rutgers University, 195 Little Albany Street, New Brunswick, New Jersey, 08903, USA.
E-mail: shenzh@cinj.rutgers.edu
[5]Current address: The First Hospital of Jilin University, Changchun, Jilin Province, China.
Received 15 September 2016; revised 11 January 2017; accepted 26 February 2017; published online 10 April 2017

In this work we demonstrate that BCCIP, especially BCCIPα, associates with centrosomes, spindle poles and the mitotic cell cortex. We identify BCCIP as a new component of the centrosome and the mitotic spindle pole, and functions in regulating microtubule anchoring, microtubule stability, spindle architecture and spindle orientation. These newly identified functions appear to be independent of BCCIP's role in DNA damage response. Our work not only identifies a critical component of the mother centriole that plays a role in interphase microtubule organization but also in dynein/dynactin-mediated spindle assembly. These data suggest an additional mechanism by which BCCIP contributes to not only genomic stability but also to organismal development.

RESULTS

Preferential localization of BCCIP to the mother centriole

BRCA2 and BRCA1 are *bona-fide* components of the microtubule-organizing center, and BCCIP has been demonstrated to interact with BRCA2.[30,33,34] In HT1080 cells, we observed a clear localization of BCCIP in both the interphase centrosome and the
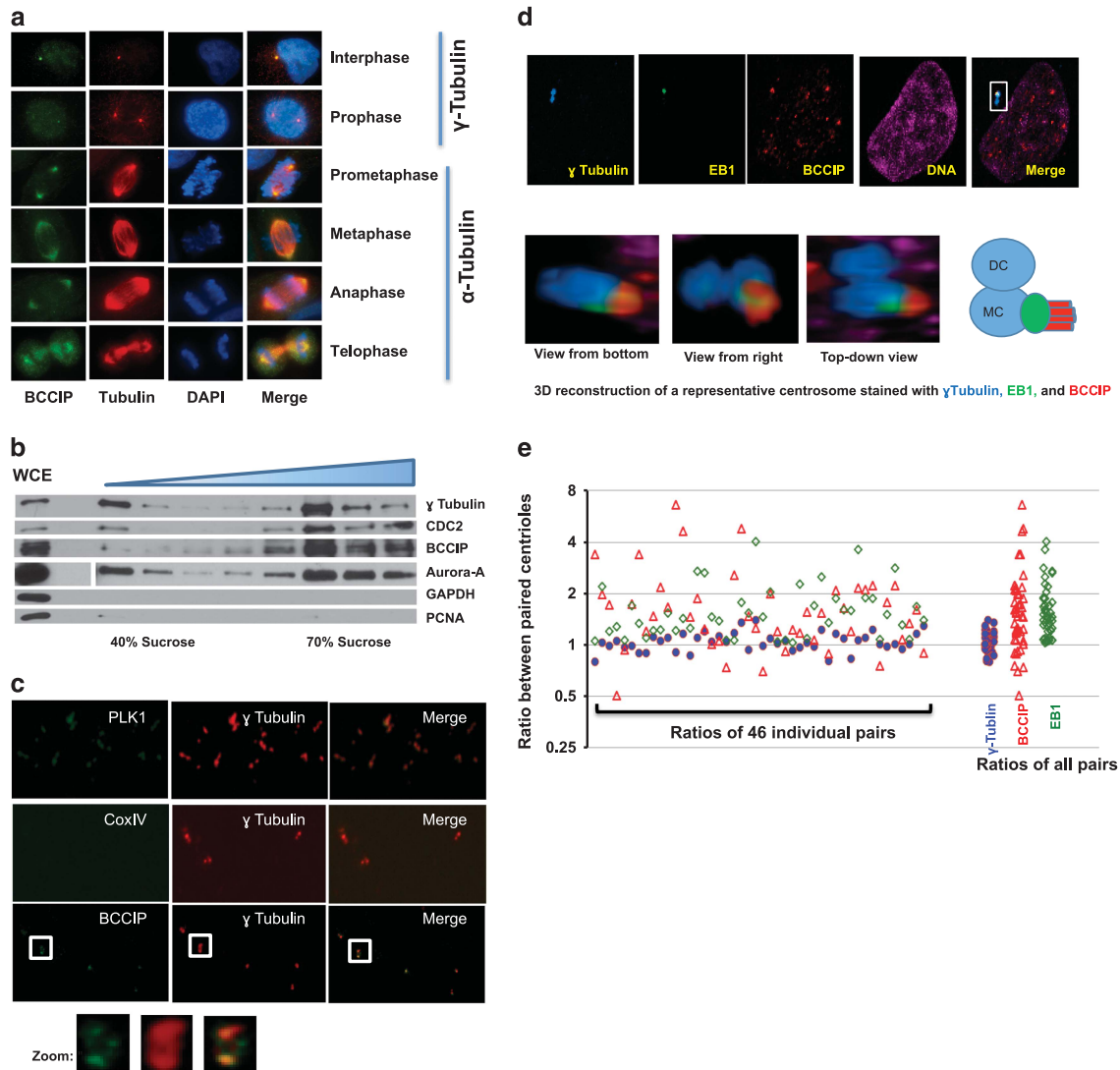

Figure 1. BCCIP is associated with the centrosome and the mitotic apparatus. (a) The localization of BCCIP to centrosomes and spindle poles. HT1080 cells were probed with anti-BCCIP and anti-γ-tubulin (interphase centrosomes; top two rows) or with anti-BCCIP anti-α-tubulin (mitotic spindles; bottom four rows). Shown are representative images of cells at indicated cell cycle phase. (b) Purification of centrosome isolates. HeLa cells were synchronized in mitosis, collected and lysed. Centrosomes were separated by sucrose gradient centrifugation (see Materials and Methods). Following density gradient centrifugation, centrosome fractions were collected, boiled in SDS sample buffer and subjected to SDS-PAGE and western blot. The assayed fractions were probed with the indicated antibodies. The concentration of the sucrose fraction increases from left to right (40–70%). WCE: whole cell extract. (c) BCCIP is associated with purified centrosomes. Centrosome isolates were pooled, sedimented onto a coverslip and immuno-probed with the indicated antibodies. The boxed image is zoomed to demonstrate the decoration of BCCIP around the orthogonal centriole pair. (d) Preferential localization of BCCIP to the mother centriole. GFP-EB1 expressing HT1080 cells were immunostained for γ-tubulin (blue, a marker equally present on both centrioles) and BCCIP (red). Images from a representative pair of centrioles as viewed from three different angles are depicted, as well as a cartoon illustrating the arrangements of γ-tubulin, EB1 and BCCIP. MC: mother centriole, DC: daughter centriole. (e) The relative distribution of proteins between paired centrioles. The fluorescent intensities of γ-tubulin, BCCIP and EB1 among 46 centriole pairs were measured. Shown are the fluorescent intensity ratios and the clustered plot of ratios among all the centriole pairs. A 3D view of the BCCIP localization to interphase centrioles and mitotic spindles can be found in Supplementary Figure S2, Supplementary Movies M1 and M2.

mitotic spindle poles as judged by BCCIP colocalization with γ-tubulin or α-tubulin (Figure 1a). Interestingly, during late prophase, immunofluorescent staining revealed that the concentration of centrosomal BCCIP was enhanced relative to interphase cells and that BCCIP appeared to expand its presence to the crescent-shaped spindle pole matrix (Figure 1a). The specificity of the BCCIP antibody was fully validated by western blots, antigen absorption followed by immunofluorescent staining (see Supplementary Figures S1a and b), and the localization of BCCIP to centrosomes was confirmed with several independent antibodies in different human and mouse cells (Supplementary Figures S1c-e).

To confirm these observations, we first purified centrosomes through use of sucrose gradient centrifugation. Following ultracentrifugation, gradient fractions were collected and the centrosome-enriched fraction was verified by immunoblotting for the centrosome markers γ-tubulin, Aurora-A and CDC2. As shown in Figure 1b, the centrosome fractions were devoid of the cytosolic and nuclear markers (GAPDH and PCNA), but enriched with several centrosome components (γ-tubulin, Aurora-A and CDC2), as well as BCCIP. Furthermore, when the centrosome fraction was centrifuged through a glycerol cushion onto a coverslip and stained for the centrosome markers PLK1 and γ-tubulin, we observed that BCCIP, but not CoxIV (a non-centrosome protein), was retained within the centrosome complex (Figure 1c).

In interphase cells, we noticed that BCCIP tended to be co-enriched with EB1 within one centriole, and was relatively reduced within its cohort (Figure 1d). In order to quantitate this phenomenon, we acquired 0.2 micron centrosome Z-stacks and measured the fluorescent intensities of γ-tubulin, BCCIP or EB1 within each centriole. We then calculated the protein fluorescent intensity ratio between the paired EB1-high (mother) and EB1-low (daughter) centrioles. As shown in Figure 1e, the distribution of γ-tubulin between the paired centrioles was relatively identical, with an average ratio and standard error values of 1.05 ± 0.02 ($n = 46$). However, the EB1 and BCCIP ratios between the same centriole pairs demonstrated values of 1.56 ± 0.08 and 1.78 ± 0.17, respectively, both significantly higher than that of γ-tubulin ($P = 6.8E-08$, $8.5E-05$, respectively, Student's t-test). These results suggest that BCCIP exhibits a localization bias within EB1-enriched mother centrioles. Three-dimensional reconstruction of the centrosome complex revealed that BCCIP sheathed, but did not overlap the appendage marker EB1 (Figure 1d, Supplementary Figure S2 and Supplementary Movie M1), which suggests that BCCIP is not a subdistal appendage component, but is more likely a physical tether between the microtubule minus-end and the subdistal appendages. Altogether, these data firmly establish that BCCIP is a component of the centrosome and mitotic spindle pole, and that most of BCCIP is confined proximal to, but not within, the subdistal appendages of the mother centriole in interphase.

The human-specific BCCIPα is the dominant centrosome and spindle pole-associated isoform, but this association is mediated through a shared domain between BCCIPα and BCCIPβ

Human cells express two isoforms of BCCIP created by alternative splicing, designated as BCCIPα and BCCIPβ.[26] These two isoforms are largely identical with the exception of a variable C terminus.[26] This discrepancy led us to ask the question whether human cells exhibited isoform-specific localization patterns. To address this question we expressed YFP-BCCIPα or YFP-BCCIPβ in cells, and were surprised to notice that BCCIPα clearly associated with spindle poles and fibers (Figure 2a), while BCCIPβ only weakly appeared on spindle poles (Figure 2a). Next, we examined the distribution and retention of BCCIP isoforms in the centrosome complex after treatments with buffers of increasing ionic strength (see Materials and Methods). As shown in Figure 2b, BCCIPα was

more abundant than BCCIPβ in the centrosome preparation. Although both isoforms could be removed from the centrosome complex with weak detergents, BCCIPα appeared to be more resistant to extraction than BCCIPβ. In contrast, core centrosome components, such as γ-tubulin and HSP90, could only be removed with harsher chaotropic reagents, as previously demonstrated.[35] Taken together, these results demonstrate that in human cells both isoforms of BCCIP are capable of associating with the centrosome and the spindle pole, but BCCIPα is the more dominant isoform. Intriguingly, the sole BCCIP isoform in mice, which resembles human BCCIPβ, can fully localize to spindle poles endogenously in mice (Supplementary Figure S1d), and when transiently expressed in human cells (Supplementary Figure S1e). These findings suggest that humans have likely evolved a preferred spindle pole-associated BCCIP isoform but in the absence of BCCIPα, BCCIPβ (or BCCIPβ-like homologs) demonstrates a comparable localization to centrosomes and mitotic spindle poles.

Next, we sought to determine the domain that mediated the localization of BCCIP to the spindle pole. To answer this question, we transiently expressed a panel of shRNA-resistant YFP-BCCIP fragments in BCCIP knockdown cells (Figures 2c and d). We observed that the smallest fragment capable of binding to the spindle pole spanned amino acids 111–257, which contains a putative and conserved coiled coil domain (Figure 2c). Deletion of either the coiled coil (BCCIP-SR3 in Figure 2c) or the region upstream of the coiled coil (BCCIP-Δ2 in Figure 2c) markedly reduced the association of BCCIP with the spindle pole. Interestingly, although BCCIPα and BCCIPβ have distinct C termini,[26] loss of the C terminus of BCCIPα had no effect on spindle pole localization. These data imply that the unique C terminal of BCCIPα does not promote its association with the spindle pole, but rather it is likely that C-terminus elements found in BCCIPβ restrict its binding, consistent with the finding that the sole mouse BCCIP isoform is able to localize to the spindle pole (Supplementary Figures S1d and e).

BCCIP is recruited to the spindle pole matrix and centrosome by microtubules and dynein/dynactin activity

The spindle pole matrix consists of a meshwork of microtubules, centrosomes, MAPs and molecular motors and depends on an intact microtubule network together with retrograde motor transport for assembly.[1,15] Conversely, centrosome core components are associated with the centrosome constitutively and do not depend on microtubule flux.[35,36] The observation that BCCIP localized to both interphase centrosomes and mitotic spindle poles (Figure 1a) prompted us to determine whether the localization of BCCIP was dependent on microtubules. To answer this question, we first challenged cells with nocodoazole, a microtubule depolymerizing agent, or taxol, a drug that inhibits the disassembly of microtubules (Figure 3a). We observed that nocodazole completely disassembled the spindle, reducing centrosomes to their respective centrioles, and eliminated most but not all of the endogenous BCCIP signal at the centrosome as visualized by colocalization with either α-tubulin or γ-tubulin staining (Figure 3a, middle row). Alternatively, taxol induced the formation of multiple psuedo-asters and abolished the tight association of the centrosomes with the minus-end of the spindle. We observed that in this condition BCCIP was strongly recruited to the taxol-stabilized microtubule bundles, but largely lost from the centrosomes (lower panel Figure 3a). Identical results were reproduced by YFP-tagged BCCIPα (Supplementary Figure S3a). Next, we recapitulated these results biochemically by precipitating microtubules from mitotic lysates with taxol and observed that both BCCIPα and BCCIPβ were enriched in the taxol-treated microtubule pellet fraction, but not in the nocodazole-treated sample (Figure 3b). In addition, transiently expressed YFP-BCCIPα
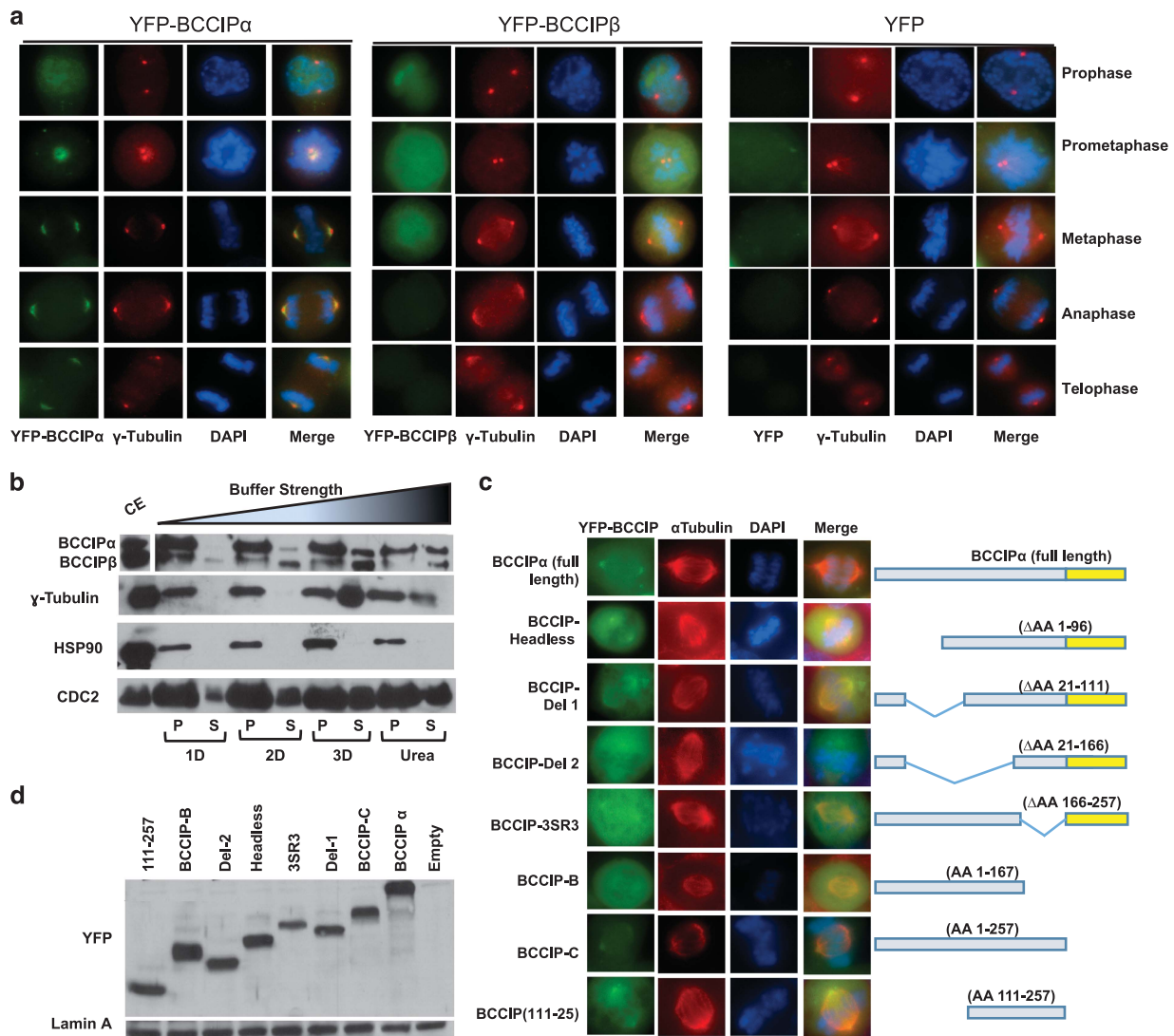
Figure 2. BCCIPα is the predominant centrosome-associated isoform. (a) The localization of exogenous BCCIP isoforms to spindle poles. HT1080 cells stably expressing YFP-BCCIPα, YFP-BCCIPβ or YFP (negative control) were stained for γ-tubulin (red, centrosomes) and counterstained with DAPI. Illustrated are the representative images at different stages of mitosis. (b) BCCIP has a labile association with centrosomes. Centrosome fractions were pelleted and incubated with the indicated buffers, re-pelleted by centrifugation and the supernatant was collected. The remaining pellet fraction (P) was resuspended in boiling loading buffer and both supernatant and pellet fractions were subjected to SDS-PAGE and western blot. The crude extract (CE) was run concurrently as reference. P: the pelleted centrosomes after buffer treatment; S: the stripped-off proteins in the solution. 1D, 2D, 3D and Urea indicate the buffers with increasing ionic strength (see Materials and Methods). (c) Amino acids 111-257 of BCCIP mediate its localization to spindle poles. The illustrated panel of YFP-tagged full-length and truncated BCCIP proteins were transiently expressed in BCCIP knockdown 293 T cells. Cells were co-probed with α-tubulin to assess spindle pole localization. (d) Expression verification of exogenous YFP-BCCIP fragments. The expression levels of the same panel of BCCIP fragments as in panel-2C verified by western blot.

and YFP-BCCIP (aa111-257), but not YFP alone, had equal affinity to microtubules (Supplementary Figure S3b), confirming a requirement for this domain to associate with the spindle pole.

We then reasoned that because the deposition of BCCIP to the poles required an intact microtubule network, BCCIP might be localized through the activities of the major minus-end motor protein dynein/dynactin, a multiprotein complex comprised of at least seven subunits, including p150 glued and Arp-1.[18,37] In order to test this hypothesis, we performed a GST pulldown of mitotic cell lysates with BCCIPα and BCCIPβ, and GST (Figure 3c). Intriguingly, BCCIPα, but not BCCIPβ or GST itself, was sufficient to pull down the dynactin components, p150 glued and Arp-1, and dynactin and BCCIP were associated with a complex that contained centrosomal γ-tubulin and α/β-tubulin dimers (Figure 3c). In addition, BCCIP and p150 glued colocalized

proximal to the mother centriole during interphase, as well as the spindle pole and cortex during mitosis (Figure 3d).

Last, to determine whether dynein activity was required for proper BCCIP targeting during mitosis, we incubated cells with the dynein-specific inhibitor Ciliobrevin-D. In this condition we observed that the normally compact focus of BCCIP at the spindle poles was broadened and increased compared to the control, suggesting that dynein motility plays a critical role in deposition of BCCIP in the cell (Figures 3e and f). To recapitulate this finding genetically we overexpressed the p50/dynamitin subunit of dynactin, which results in a well-characterized dominant-negative dispersion of the dynactin complex and subsequent inhibition of the retrograde transport of dynactin cargo.[15,38] We found that transient overexpression of the dynactin subunit p50/dynamitin markedly disrupted the spindle pole-associated BCCIP fraction
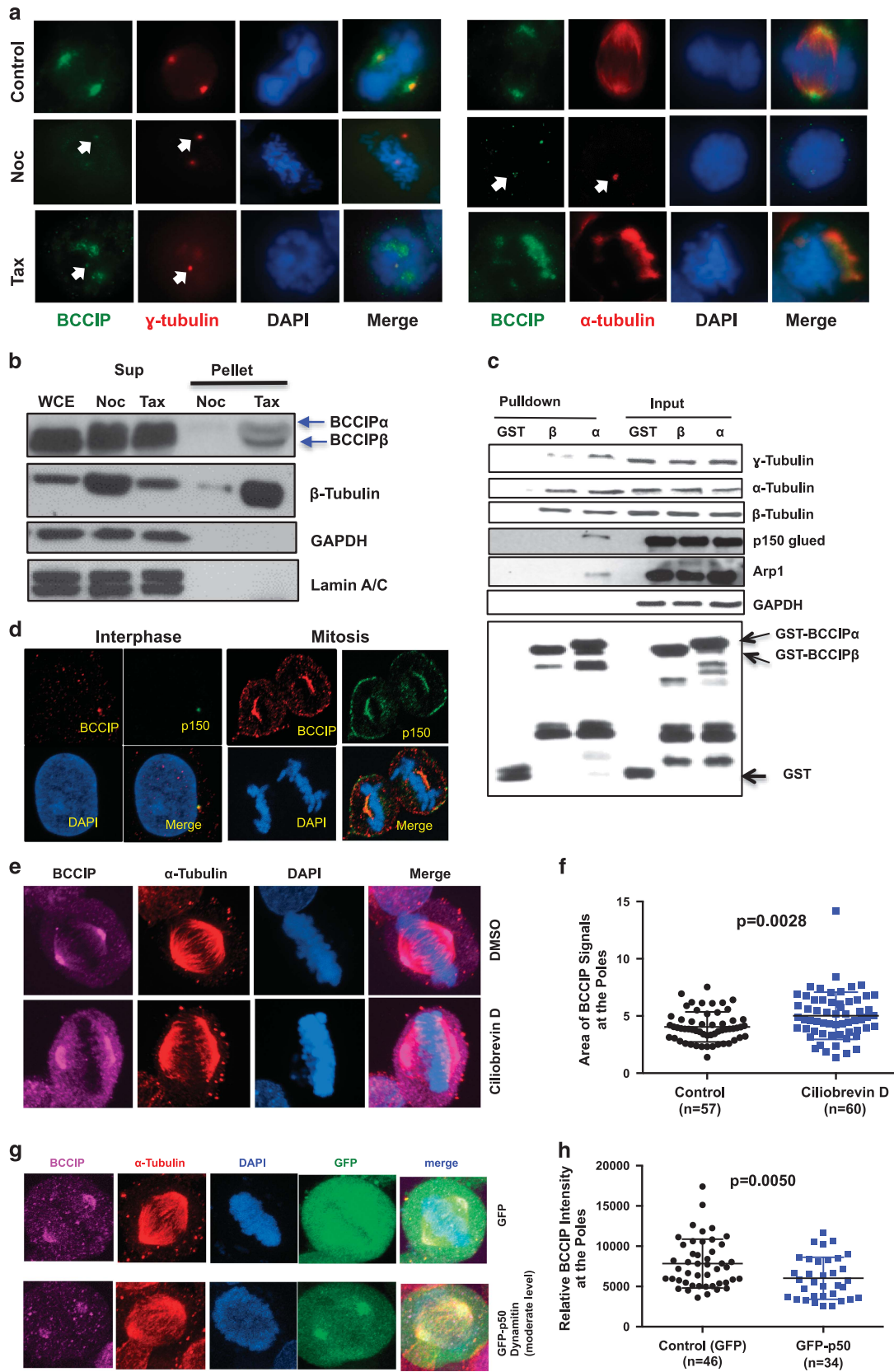
(Figures 3g and h), suggesting a model where BCCIP associates with dynein/dynactin in a microtubule-dependent manner.

BCCIP is required for the microtubule organization at the spindle pole and centrosome

The formation of the microtubule array is comprised of the following three independent but interconnected steps: first the nucleation of nascent tubulin by γ-tubulin complexes, second the elongation, stabilization and minus-end capping of the microtubule polymer by minus-end-associated MAPs, and third the anchoring of the growing microtubule to the subdistal appendages of the mother centriole.[39,40] We then hypothesized that constitutively associated centrosome fraction of BCCIP might be involved in the regulation of minus-end microtubule dynamics, given that BCCIP also associates with microtubules. In order to test this hypothesis, a microtubule regrowth experiment was performed. We first treated mitotic cells with nocodazole over ice to depolymerize microtubules followed by washout with prewarmed media to promote microtubule regrowth. We observed no remarkable difference in the microtubule nucleation stage of regrowth (5-min recovery) in BCCIP-deficient cells. Consistent with this finding, levels of the microtubule nucleating factors γ-tubulin and pericentrin were identical at the poles in control and BCCIP knockdown cells (data not shown). Despite this result, as shown in Figures 4a and b, after 30 min of recovery, while most of the control cells were able to form a well-focused bipolar spindle, BCCIP-deficient spindles remained unorganized and contained a diminished amount of spindle microtubules. To further confirm this finding, we then filmed GFP-tubulin expressing control and BCCIP knockdown cells after overnight treatment with nocodazole and a 1-h cold shock. We observed that following recovery, a bipolar spindle was re-established at roughly 40 min in control cells, whereas this number was increased to 70 min ($P = 0.033$) in BCCIP-deficient cells (Figure 4c). These data strongly demonstrate that BCCIP deficiency compromises spindle assembly independent of microtubule nucleation.

Next, because BCCIP is localized to proximal to the mother centriole and binds dynactin, a microtubule-anchoring factor,[18,19] we hypothesized that the interphase centrosomal fraction of BCCIP might be involved in microtubule organization. In order to test this hypothesis, we then seeded a mixture of GFP-tagged BCCIP knockdown and wild-type (GFP negative) cells onto the same coverslip, and verified that the BCCIP normal and BCCIP knockdown cells could be readily distinguished based on the GFP signals on the same slide (Figure 4d). Cells were then treated identically to Figure 4a and b. This approach was adapted to eliminate potential sampling bias due to the fast nature of microtubule regrowth in interphase cells. As shown in Figures 4e and f, asters of roughly equal intensity formed in both control and BCCIP-deficient cells at 2 min, demonstrating that BCCIP depletion does not impact centrosome nucleation, mirroring our findings during mitosis. However, at 5 min after recovery, the microtubule intensity around each centrosome was significantly reduced in BCCIP-deficient cells. This delayed reformation of microtubule was recovered by 20 minutes, but in this state we observed that a significant portion of BCCIP-deficient cells exhibited abnormal morphology (Figure 4f, 20 min), and lacked a sharply focused radial array of centrosome microtubules (Figures 4g and h). These data (Figures 4d–h) suggest that interphasic BCCIP-deficient cells are defective in organizing microtubules, and suggest that BCCIP fulfills a role in the regulation of microtubule anchorage/ organization.

BCCIP deficiency reduces tubulin acetylation

Microtubule growth from the centrosome is a multistep process that involves the coordination of nucleating complexes, minus-end-associated MAPs and centrosomal anchoring proteins.[11] Because the organization of centrosomal microtubules was affected by BCCIP depletion, we theorized that BCCIP might also have a microtubule stabilizing role.[14] Such a case has previously been observed in the p150 subunit of dynactin, an anchoring factor that also regulates microtubule stability.[20] K-40 acetyl-tubulin has been regarded as a surrogate marker for stable microtubules,[20,41–43] and thus we chose to examine the K-40 acetylation status in control and BCCIP-deficient cells. As shown in Figure 5a, BCCIP loss resulted in a loss of K-40 acetyl-tubulin in both BCCIP knockdown HeLa cells and in MEF cells where BCCIP had been deleted. To verify the reduction of acetyl-tubulin in BCCIP knockdown cells, control and BCCIP knockdown HeLa cells were mixed at 1:1 ratio and costained with acetyl-tubulin and BCCIP on the same slide. As shown in Figure 5b, the BCCIP-deficient cells (with weak green signals) had a significantly lower level of acetyl-tubulin (red signal) than the BCCIP-proficient cells (with strong green signals and arrowed) had in the same field.

To further address which specific isoform of BCCIP resulted in a loss of acetyl-tubulin, we then expressed shRNA-resistant YFP-BCCIPα, YFP-BCCIPβ or YFP in BCCIP knockdown cells (see Supplementary Figure S4 for representative images), and compared the relative intensity of acetyl-tubulin with the knockdown or control cells. As shown in Figure 5c, the BCCIP knockdown cells demonstrated reduced levels of acetyl-tubulin compared to wild-type cells. YFP-BCCIPα, but not YFP-BCCIPβ or YFP, was capable of recovering this marker (Figure 5c). These data suggest that BCCIP, particularly BCCIPα, confers microtubule stability.

Figure 3. BCCIP binds to microtubules and is recruited to spindle poles by dynein/dynactin activity. (**a**) The localization of BCCIP to spindle poles requires microtubules. U2OS cells were treated with nocodazole or taxol and were co-stained with BCCIP and γ-tubulin (left group) or with BCCIP and α-tubulin (right group). When the spindle is depolymerized by nocodazole, α-tubulin stains the nocodazole-resistant centriole microtubules. The arrows indicate the small fraction of BCCIP that remains stably associated with centrosomes following treatments. (**b**) BCCIP co-precipitates with polymerized microtubules. Mitotic cell lysates were precleared by ultracentrifugation. The soluble lysates were then treated with taxol (Tax) to repolymerize microtubules or nocodazole (Noc) to prevent repolymerization. Following ultracentrifugation, microtubules are in the pellet (P), and soluble tubulin is retained in the supernatant (S). Equal portion of supernatant and pellet fractions were subjected to western blot and with the indicated antibodies. Sup: supernatant; WCE: whole cell extract; N: Nocodazole treated; T: Taxol treated. (**c**) BCCIP complexes with microtubules, centrosomes and dynactin. HeLa mitotic extract was incubated with GST-BCCIPα, GST-BCCIPβ or GST and subjected to glutathione-bead pulldown. 1% of the input and 5% of the pulldown was subjected to western blot and probed with the indicated antibodies. (**d**) BCCIP co-localizes with dynactin at the mother centriole, spindle pole and cell cortex. Shown are representative confocal images demonstrating the colocalization of BCCIP with dynactin at the mother centriole during interphase and the spindle pole and cell cortex during mitosis. (**e, f**) Inhibition of dynein by Ciliobrevin-D disrupts the distribution of BCCIP at the spindle poles. U2OS cells were treated with the dynein inhibitor Ciliobrevin-D and stained with the indicated antibodies. Shown are the representative images (**e**) and the quantified BCCIP-positive areas from spindle poles (**f**). (**g, h**) Overexpression of p50/dynamitin diminishes the levels of spindle pole-associated BCCIP. HeLa cells were transfected with GFP-p50/dynamitin or GFP, and the BCCIP intensity at the poles was quantified. Shown are representative images (**g**) and quantification of the BCCIP intensity at the poles.
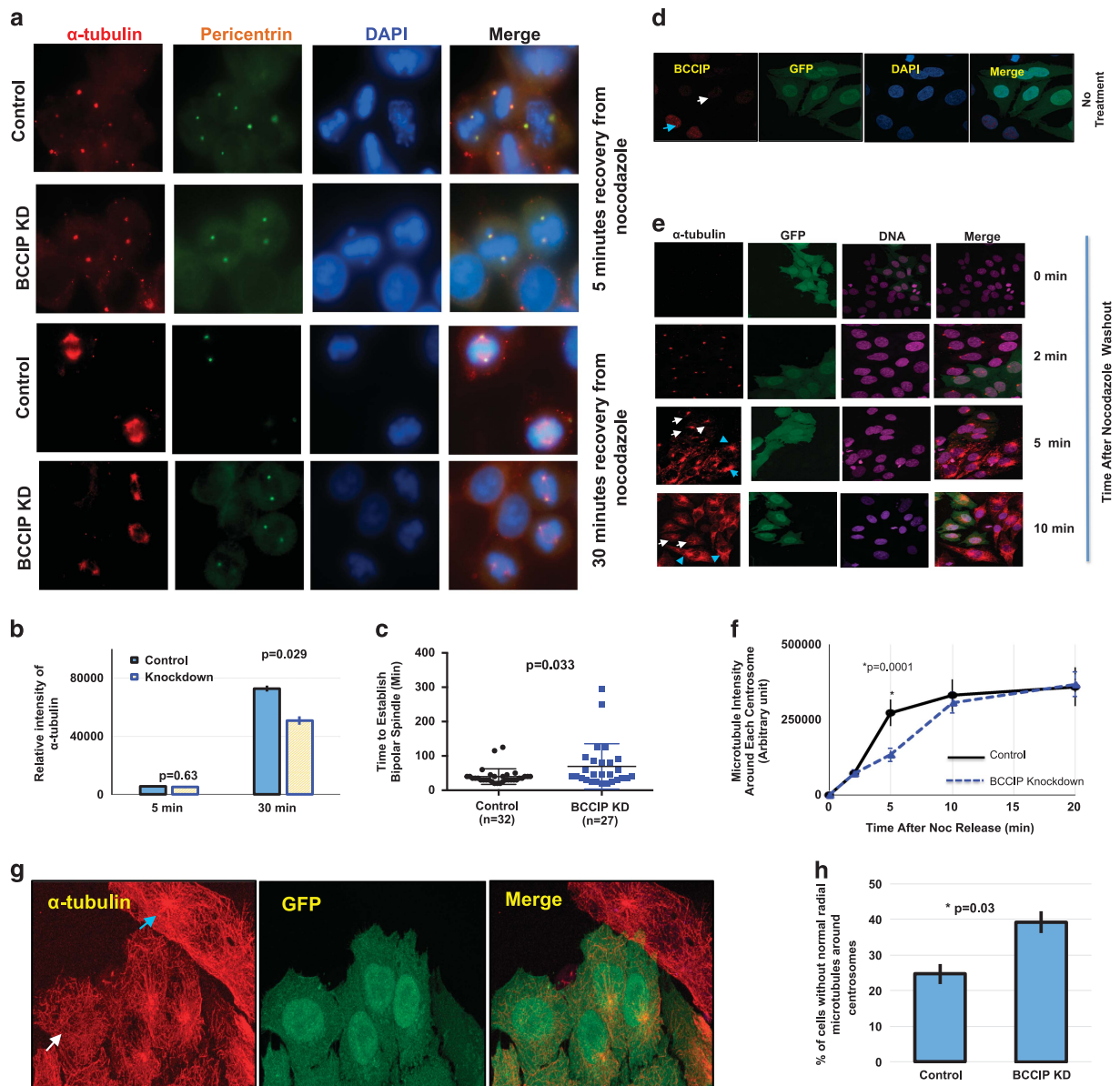
Figure 4. BCCIP loss negatively impacts microtubule retention. (**a**–**c**) Recovery of mitotic spindle formation after nocodazole treatment. Control and BCCIP knockdown cells on different slides were treated with nocodozole, washed and allowed reformation of spindles. (**a**) and (**b**) are the representative image sets and the quantified α-tubulin intensity at 5 and 30 min after recovery from nocodazole treatment, respectively. (**c**) is the time used to re-establish bipolar spindle after nocodazole washout are quantified using time-lapse analysis from individual mitotic control or BCCIP knockdown cells. (**d**–**h**) Recovery of interphase centrosome microtubule after nocodazole treatment. Control and GFP-labeled BCCIP knockdown cells are mixed and seeded on the same coverslip, immunofluorescent staining was performed at indicated times after washing off the nocodazole treatment, and the intensity of α-tubulin in GFP-positive (BCCIP knockdown) and GFP-negative (BCCIP normal) cells was measured and compared. (**d**) shows the verification of distinguishable BCCIP levels between GFP-negative (control) and GFP-positive (BCCIP knockdown) cells by anti-BCCIP staining in interphase cell. The blue arrowhead indicates a representative GFP-negative control cell expressing normal levels of BCCIP, and the white arrow indicates a GFP-positive cell with BCCIP knockdown. (**e**) are representative images of α-tubulin intensity in control (GFP-negative) and knockdown (GFP-positive) cells at indicated times after nocodazole washout and recovery. Blue arrowheads indicate centrosomal α-tubulin intensity in control cells while white arrows indicate centrosomal α-tubulin intensity in GFP-positive BCCIP knockdown cells. (**f**) is the quantified intensity of α-tubulin following recovery from nocodazole. The α-tubulin signal was quantified in predetermined area around each centrosome in control and BCCIP knockdown cells and plotted at the indicated time points. (**g**) are representative images of a control cell (blue arrowhead) that exhibit a well-formed radial microtubule organization, adjacent to a BCCIP knockdown cell (white arrow) that lacks a normal radial microtubule focus. (**h**) shows the percentages of interphase cells lacking a normal radial microtubule organization (unfocused microtubules) as represented in (**g**). Depicted are data obtained from 232 control and 259 knockdown cells.

Spindle defects in BCCIP-deficient cells

Dynein, dynactin and spindle pole auxiliary proteins, such as NuMa, play an essential role in mitosis by regulating spindle length, architecture and positioning.[8,9,18] The association between BCCIP and dynactin components, together with the spindle pole localization of BCCIP (Figure 3c), led us to ask the question whether BCCIP loss resulted in mitotic spindle defects. First we investigated the architecture of the mitotic spindle in BCCIP-deficient cells. As shown in Figure 6a, the spindles in BCCIP-deficient HeLa cells appeared bipolar, but collapsed, leading to a
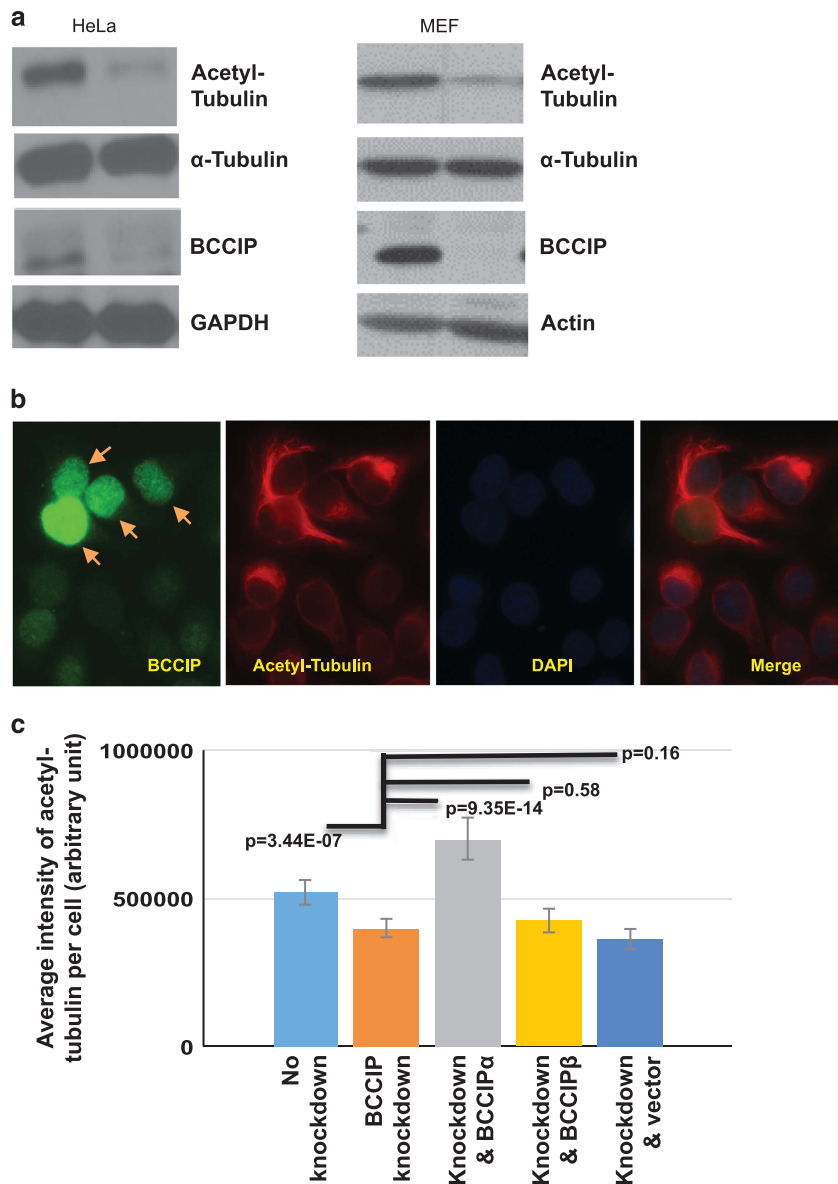
Figure 5. BCCIP deficiency decreases levels of stable, acetylated microtubules. (**a**) BCCIP knockdown reduces microtubule acetylation. Control and BCCIP knockdown HeLa cells or MEF control and MEF BCCIP knockout cells were lysed and blotted for the stable microtubule marker, acetyl-tubulin. (**b**) Levels of acetylated-tubulin in control and BCCIP knockdown cells. HeLa cells expressing BCCIP-shRNA (weak green, un-arrowed) were mixed with control cells (strong green, arrowed), and stained for BCCIP and acetyl-tubulin. (**c**) The reduced acetyl-tubulin in BCCIP-deficient cell can be rescued by RNAi-resistant BCCIPα. RNAi-resistant YFP-BCCIPα, YFP-BCCIPβ and YFP were re-expressed in BCCIP knockdown cells. These YFP-positive cells were mixed with non-transfected knockdown or control cells (YFP-negative cells). Total fluorescent intensity of acetyl-tubulin in BCCIP knockdown (YFP-negative) and BCCIP re-expressed (YFP-positive) cells on the same staining slide was quantified. Shown are relative intensities of acetyl-tubulin in wild-type cells (first column from left), BCCIP knockdown cells (second column from left) and the knockdown cells expressing different YFP-tagged proteins. Representative images of rescue can be viewed in Supplementary Figure S4.

reduced pole-to-pole distance (Figure 6b). Close examination of the minus end of BCCIP-deficient spindles revealed a broadening at the poles, and the normally sharp focus at the minus end of the spindle was stretched in BCCIP-deficient cells (Figure 6a). Additionally the spindle arc angle (see orange arc in Figure 6a cartoon), or the angle between the distal points of the spindle microtubules, was significantly widened at the spindle poles (Figures 6a and c) and spindle pole components were stretched and splayed in BCCIP-deficient cells (see green line in Figure 6a cartoon, and Figure 6d). These defects were also observed in BCCIP knockout MEF cells, which displayed a similar spindle pole broadening phenotype and exhibited extreme spindle pole fragmentation (bottom row of Figure 6a). These abnormalities canonically match defects in microtubule focusing and the phenotype that results from loss of dynein/dynactin/NuMa-associated activities.[8,9,18,38]

Disorientation of spindles in BCCIP-deficient cells

Dynein/dynactin cooperates with spindle pole components such as NuMa to direct motor force from the spindle pole to the cell cortex, which in turn properly orients the spindle.[8] This process plays a critical role in the fate of nascent cells during tissue regeneration and maintains stemness during asymmetric cell division.[9] We hypothesized that, because the dynein network plays an essential role in spindle orientation,[8] BCCIP silencing might confer similar defects. In order to test this hypothesis, we

immunostained cells for pericentrin and analyzed 0.2 micron Z-stacks of the spindle poles with respect to the Petri dish plane. Next, we calculated the three-dimensional tilt of mitotic spindles using the geometrics illustrated in Figure 7a. We observed that control metaphase cells typically exhibited a small spindle angle,
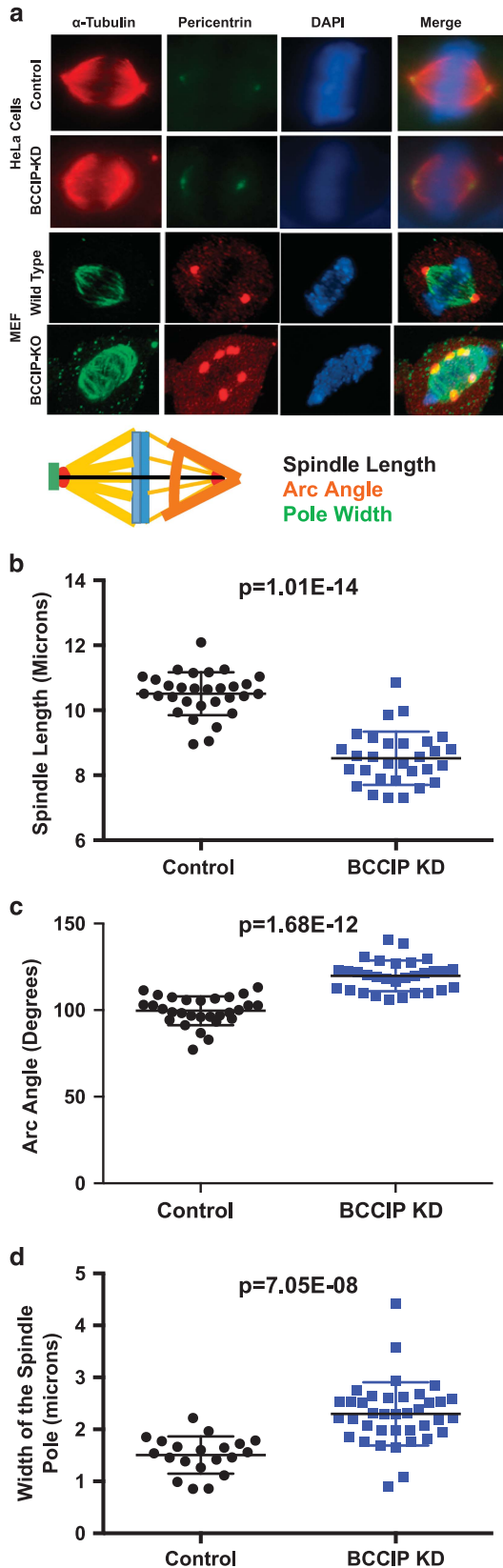
and cells were oriented so that division occurred completely parallel to the culture dish surface (Figure 7b). As demonstrated in the representative images (Figure 7b), the two spindle poles (pericentrin foci) of control cells reached maximum intensity within the same confocal plane, indicating that both poles exhibited a limited angle between them. In stark contrast to the control cells, the BCCIP-deficient cells exhibited pericentrin foci that resided in two distant confocal planes. Representative 3D images of spindle orientation can be found in Supplementary Figure S5 Supplementary Movies M3 and M4. As quantified in Figure 7c, the spindle angles of BCCIP-deficient spindles were significantly increased in comparison to those in the control, suggesting that the BCCIP deficiency imparts spindle orientation defects. In order to determine whether this phenotype was specifically induced by loss of BCCIPα, we then performed a rescue experiment by re-expressing shBCCIP-resistant flag-BCCIPα, BCCIPβ or empty vector in BCCIP knockdown cells (Figure 7b, bottom three rows). We observed that the defect in spindle orientation was largely rescued by BCCIPα expression but not by BCCIPβ (Figure 7c, Supplementary Figure S5, Supplementary Movies M5–M7), confirming that it is the BCCIPα isoform that is required for maintaining proper spindle orientation. These spindle orientation defects were further verified by time-lapse imaging, which revealed that a significant portion of BCCIP-deficient cells completed division in a manner in which one daughter cell tended to reside outside the focal plane of its cohort (see Supplementary Figure S6a).

A fraction of mitotic dynein/dynactin is deposited to the cell cortex, and this deposition is essential to produce the motor force that buttresses and orients the spindle.[8,16,21] The abnormal organization of the mitotic spindle in BCCIP-deficient cells together with the cortical localization of BCCIP (Figure 3d) led us to ask the question whether cortical dynactin was mislocalized in BCCIP-deficient mitotic cells. We first observed that BCCIP-deficient spindles were often severely displaced from their normal central distribution within the mitotic cytoplasm (Supplementary Figures S6b and c), which is indicative of astral microtubule defects.[44] Next, we investigated whether this phenotype was concomitant with misdistribution of cortical dynactin. As shown in Figure 7d, BCCIP-deficient cells demonstrated a decreased level of dynactin at the cell cortex. Thus, it is likely that the disorganization of the microtubule network in BCCIP-deficient cells also results in aberrant trafficking of dynein/dynactin and displaces it from the cortex, which in turn leads to spindle orientation defects.

Lagging chromosomes and reduced kinetochore tension in BCCIP-deficient cells

Mitotic chromosomes are aligned at the metaphase plate before the onset of anaphase. This alignment is critical for ensuring the equivalent distribution of sister chromatids into two identical daughter cells. Spindle pole focusing defects have been demonstrated to impair chromosome congression as a result of displacing pole-directed motor force, and silencing of the dynein epistasis group leads to decreased spindle tension, chromosome congression defects and delayed mitotic completion.[15,16,37,45,46] Inspection of the mitotic chromosomes in BCCIP-deficient

Figure 6. Abnormal spindle architecture in BCCIP-deficient cells. BCCIP knockdown HeLa or BCCIP knockout MEF cells were immunostained with α-tubulin and pericentrin and analyzed at metaphase. The distance between the paired centrosomes, the angles of spindle arcs and the width of the spindle poles were assessed. Representative image sets and a cartoon illustration of the assessed geometric measurements are shown in (**a**). The distributions and averages of the spindle length, arc angles and the width of the spindle poles are shown in (**b**–**d**), respectively.
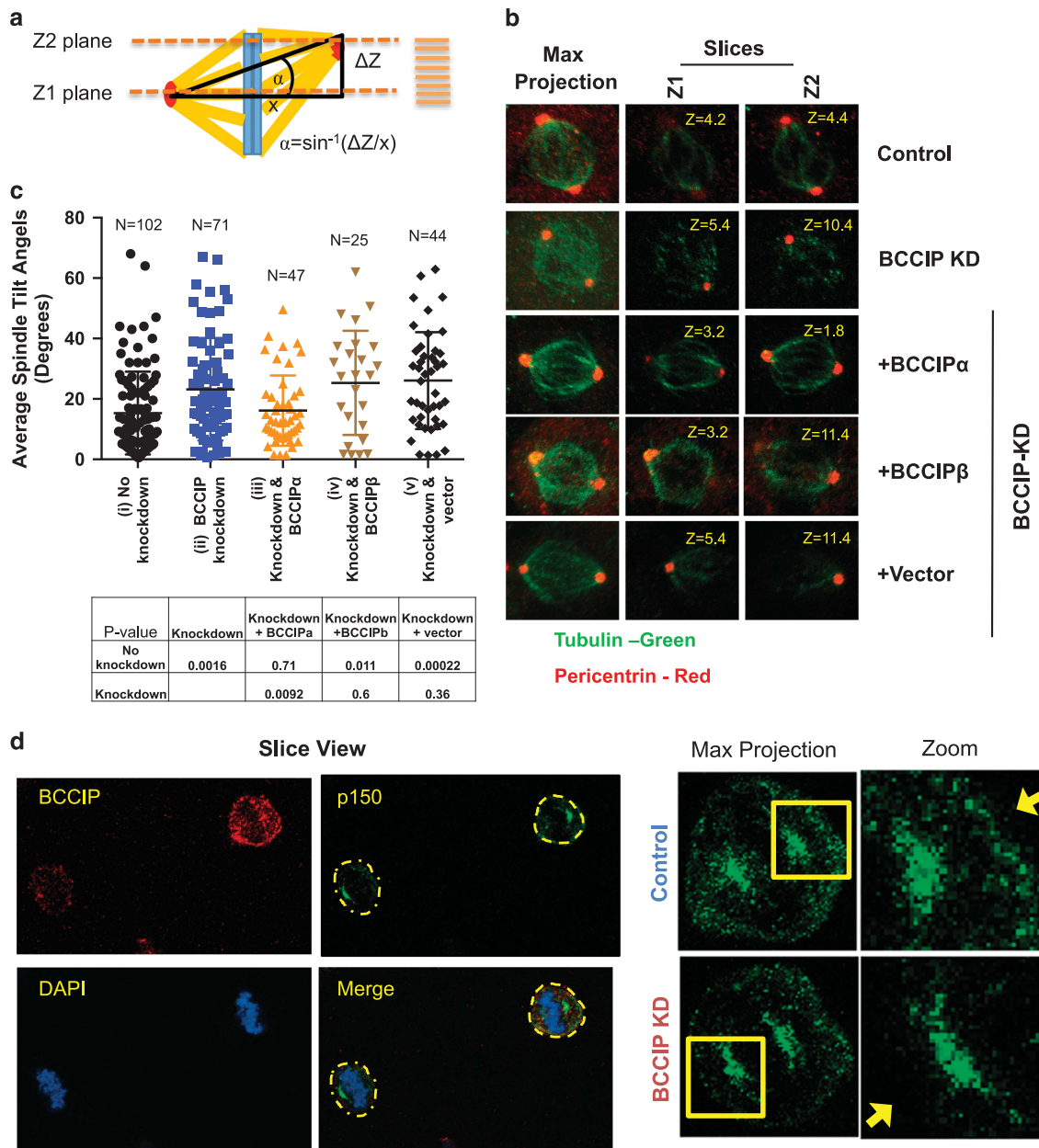
Figure 7. BCCIP loss induces spindle orientation defects. (**a**) Measurement of spindle angles. Image stacks of mitotic HeLa cells grown parallel to the culture surface were obtained by confocal imaging. The Z-planes containing maximal spindle pole intensities were recorded as Z1 and Z2, and the Z-distance between Z1 and Z2 was used to measure the depth (or the vertical distance) between the spindle poles (ΔZ shown in illustration). Maximal projections were utilized to determine the horizontal distance between the spindle poles (x-value as illustrated). Consequently, the spindle angles relative to the culture surface can be determined as $\alpha = \mathrm{Sin}^{-1}(\Delta Z/x)$. (**b**) Representative images of spindle pole planes (Z1 & Z2). Spindle poles (pericentrin foci) reside in the same Z-planes in control cells but often reside in two different confocal planes (Z1 or Z2) for BCCIP-deficient cells, reflecting an increase in the spindle angle. (**c**) The distribution of spindle angles is increased by BCCIP depletion. The spindle angles from control (i), BCCIP knockdown (ii) and knockdown cells expressing RNAi resistant BCCIPα (iii) or BCCIPβ (iv) or control vector (v) were assessed. Plotted are the distributions of the spindle angles among indicated cells. The *P*-values of *t*-test between the two indicated pairs are shown in the table. (**d**) Reduced levels of cortical dynactin in BCCIP-deficient cells. Control and BCCIP-deficient HeLa cells were co-seeded to coverslips, arrested in metaphase with MG-132 and co-stained with p150 glued (green) and BCCIP (red). Shown are the representative images of BCCIP normal (up right corner) and BCCIP knockdown (lower left corner) cells on the same staining field, and the zoomed images demonstrating the p150 staining at the spindle pole and the cortex. Yellow arrows indicate the presence (control) or lack (BCCIP knockdown) of cortex p150 staining in the control and BCCIP-deficient cells.

metaphase cells demonstrated that 24% (10 out of 41) knockdown cells contained lagging chromosomes; chromatin bodies completely disassociated from the metaphase plate. These lagging chromosomes were undetected among the control cells (0 out of 52). Next, in order to quantify chromosome alignment, we measured the chromosome congression index—a representation of the cell's ability to capture and move chromosomes.[44] We found that BCCIP knockdown significantly increased the congression index, indicating poor metaphase chromosome alignment. These chromosome congression defects were rescued by re-expression of RNAi-resistant BCCIP proteins (Figures 8a and b). We then reasoned that these defects could be resultant from two
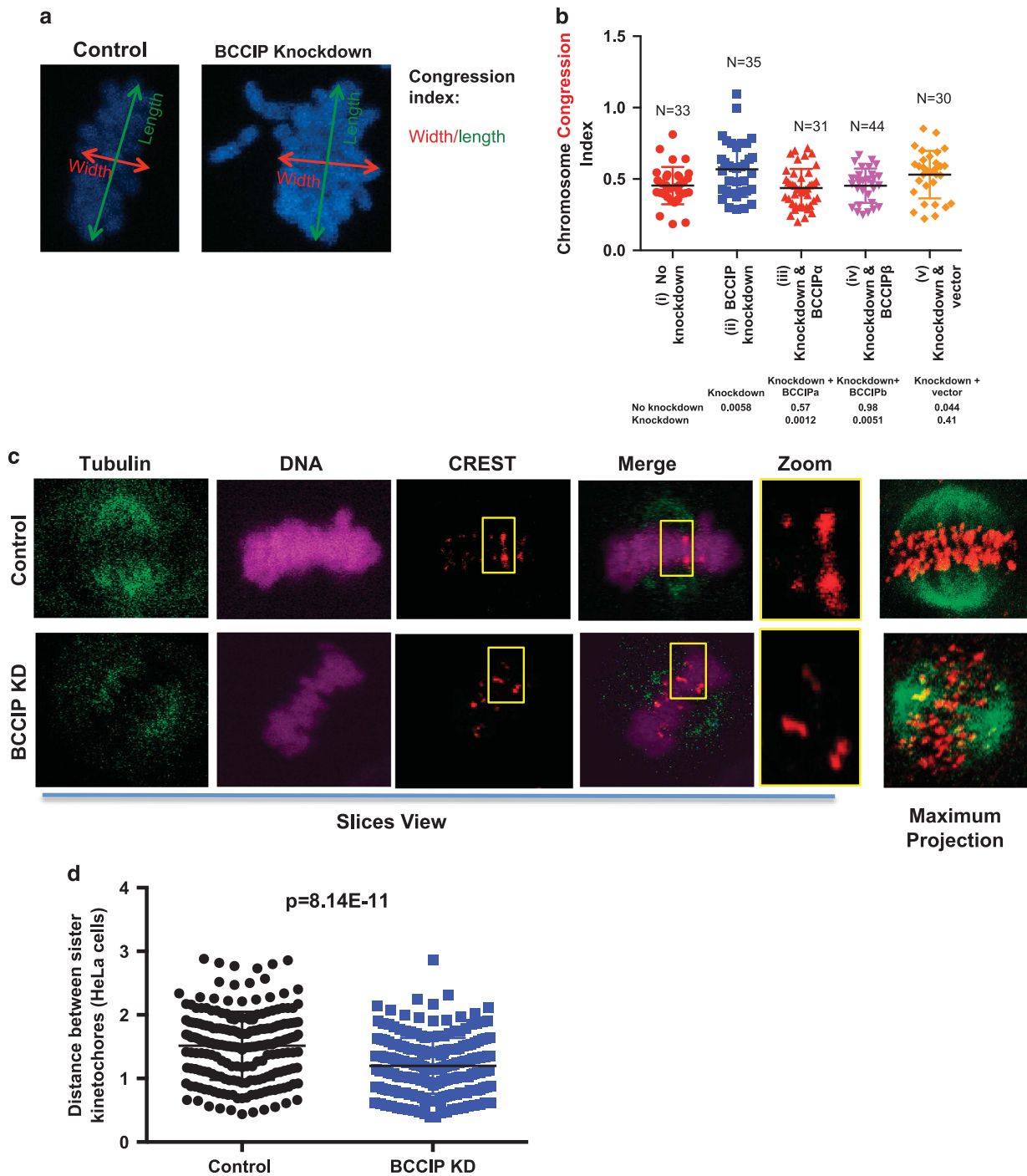
Figure 8. The forces required for chromosome movement are defective in BCCIP-deficient cells. (**a**, **b**) Abnormal congression of metaphase chromosomes in BCCIP-deficient cells. Metaphase chromosome width (parallel to the spindle poles) and length (perpendicular to the spindle poles) was obtained as illustrated. The ratio between the width and length was utilized to calculate the chromosome congression index (W/L) and plotted in (**b**) for control (i), BCCIP knockdown (ii) and knockdown cells that express RNAi-resistant BCCIPα (iii) or BCCIPβ (iv) or control vector (v). The *P*-values of *t*-test between selected cells are shown in the table below the graphic. (**c**, **d**) Reduced intra-kinetochore distance in BCCIP-deficient cells. Cells were stained with CREST (red) and α-tubulin (green). Unambiguous kinetochore CREST pairs were identified, and the distance between CREST foci (representing the distance between sister-chromatid kinetochores) was measured. (**c**) shows the representative slice views of control and BCCIP knockdown HeLa cells, a pair of identified sister bivalents (boxed and zoomed), and the maximum projections depicting accumulation of α-tubulin and CREST stacks of the confocal slice views. (**d**) illustrates the distance distribution based on measurement of more than 200 pairs. Results using U2OS cells can be found in Supplementary Figure S7.

distinct possibilities—defective poleward pulling forces or defective kinetochore microtubule attachments. We first measured spindle tension, which represents the ability of the cell to generate the robust poleward pulling forces necessary to move

chromosomes. Spindle–kinetochore tension can be represented by the distance between sister kinetochore pairs; the greater the distance between sister kinetochore foci the greater the amount of tension transduced by the spindle.[47–50] Therefore, we utilized
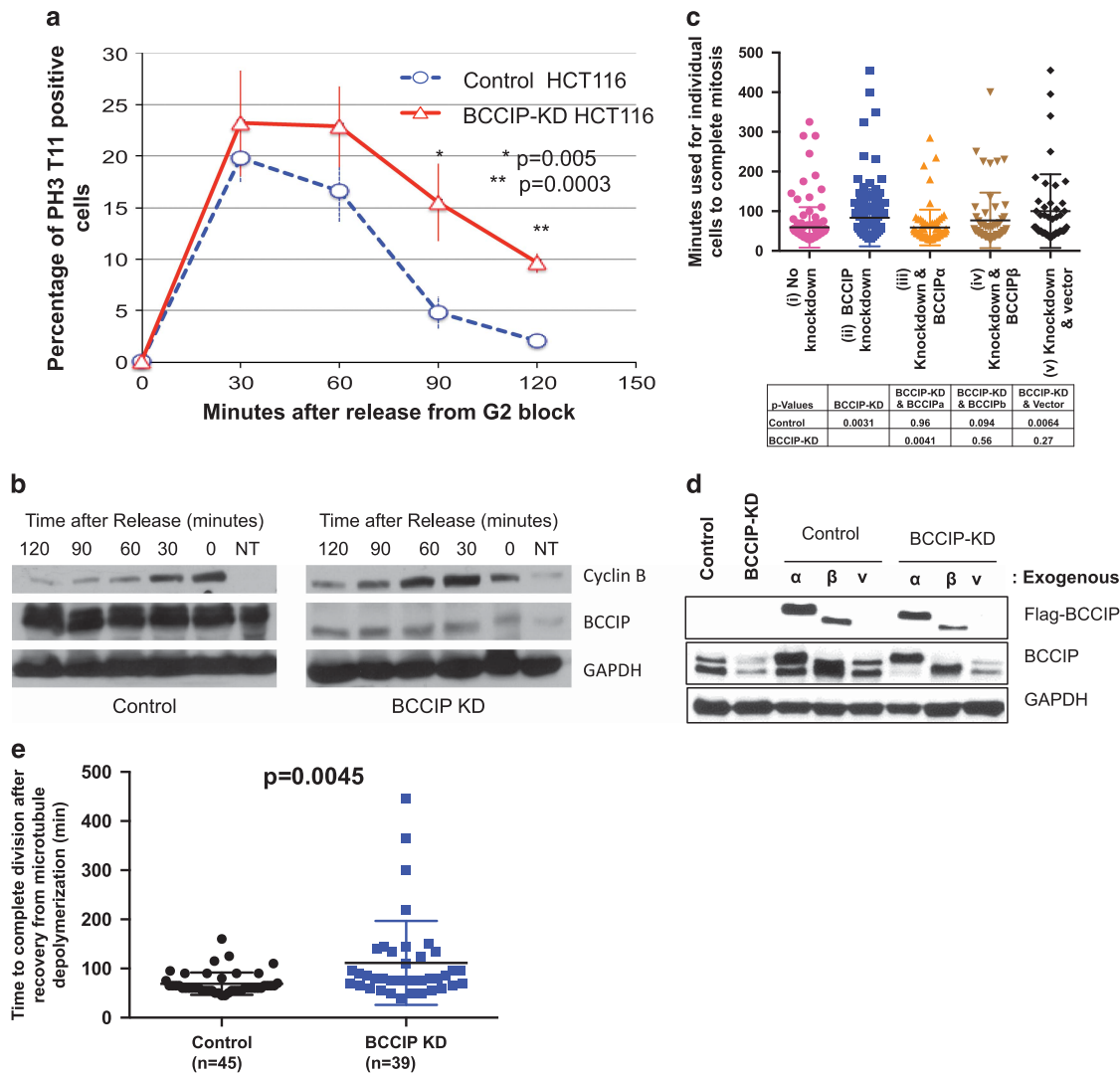
Figure 9. Delayed mitotic completion in BCCIP-deficient cells. (**a**, **b**) BCCIP loss delays anaphase onset. HCT116 cells were blocked at the G2/M boundary by RO-3306 treatment, released and immunostained with pH3-T11. (**a**) shows the percentages of mitotic cells at different times after the release from the G2/M block. (**b**) depicts a separate set of experiments where cells were blocked in M phase with nocodazole, released and subjected to western blot at the indicated time points. NT: untreated asynchronized cells used as a loading reference. (**c**, **d**) Delayed completion of mitosis in BCCIP-deficient cells. U2OS cells were filmed overnight in an incubated live cell microscope. Frames were acquired every 5 min, and the length of mitosis was quantified from the onset of nuclear envelope breakdown to the formation of a visible mid-body. Shown in (**c**) is mitotic time in control (i), BCCIP knockdown (ii), and knockdown cells rescued with RNAi-resistant BCCIPα (iii) or BCCIPβ (iv) or control vector (v). The P-values of t-test between the indicated cells are shown. Verification of the re-expression of exogenous BCCIP in the BCCIP knockdown cells is shown in (**d**). (**e**) BCCIP deficiency synergizes with spindle poison to delay in mitotic completion. Control and BCCIP knockdown HT1080 cells were treated with nocodazole over ice to completely depolymerize the mitotic spindle. The cells were then washed rapidly three times with warm media and filmed until mitosis was completed.

the distance between sister kinetochores as a surrogate for spindle tension, using the well-established method of Waters et al.[49,50] We observed a significant decrease in the distance between sister chromatid CREST foci in BCCIP knockdown HeLa (Figures 8c and d) and U2OS cells (Supplementary Figures S7a and b), demonstrating that BCCIP deficiency compromises robust pulling forces, which is consistent with the notion that BCCIP functions in coordination with dynein/dynactin/NuMa (Figure 3).[9,38] We then challenged BCCIP-deficient and control cells with a 10-min cold shock using the reported procedure.[44] This procedure is sufficient to destabilize all microtubules except kinetochore-associated microtubules (stable k-fibers), unless these attachments were rendered unstable.[44] This assay revealed no change to k-fiber stability in BCCIP-deficient cells (data not

shown), indicating that microtubule–kinetochore attachments occur normally during BCCIP silencing. Taken as a whole, these results indicate that the chromosome movement is defective in BCCIP-deficient cells.

Delayed completion of mitosis in BCCIP-deficient cells

We then predicted that the defects in spindle and chromosome geometry in BCCIP-deficient cells might lead to impaired mitotic progression. To verify this, we utilized the reversible CDK-1 inhibitor RO-3306 to synchronize BCCIP-deficient and BCCIP-competent cells at the G2/M boundary overnight. Following incubation, cells were released from the block, and fixed stepwise at different time points following the release. Mitotic cells were judged by staining with the pre-anaphase marker pH3-T11, which

4762

is rapidly dephosphorylated upon anaphase onset. We observed that BCCIP deficient and control cells entered mitosis at roughly the same rate (Figure 9a), suggesting that mitotic entry is not impeded by BCCIP loss, which is consistent with a previous report.[26] However, at the 90- and 120-min time points following release from the block, control cells roughly returned to their baseline levels of mitosis while BCCIP knockdown cells remained in M-phase (Figure 9a). These data demonstrate that BCCIP-deficient cells have a delay in mitosis, and that this delay occurs during metaphase. To verify this finding, we performed a similar experiment, but substituted RO-3306 by nocodazole to block cells in mitosis, collected lysates from control and knockdown cells after drug washout and subjected the lysates to western blot for cyclin-B, another mitotic marker that is rapidly degraded upon anaphase onset.[51,52] As shown in Figure 9b, levels of cyclin-B level peaked at 0–30 min and thereafter sharply decreased in control cells, whereas in knockdown cells the peak cyclin B fractions shifted between 30 and 60 min and reduced at a slower rate. We then used live-cell imaging to determine the precise defects observed in BCCIP-depleted cells. We generated stably expressing GFP-tubulin cell lines and observed the duration of mitosis from nuclear envelope breakdown to the formation of a visible mid-body. Cells were then transduced with empty control lentiviral particles or particles expressing shRNAs specific to BCCIP. We observed that the mitotic time was significantly extended in knockdown cells, and re-expression of BCCIPα, but not BCCIPβ or empty vector, could largely rescue the extended mitotic time in the BCCIP knockdown cells (Figure 9c). Representative time-lapse images for mitosis are shown in Supplementary Figure S8 and Supplementary Movies M8A, B and M9A, B.

To further confirm that the mitotic delay experienced by BCCIP-deficient cells was specifically due to improper spindle assembly, we disassembled spindle microtubules with nocodazole treatment and cold shock, washed the drug away with warm media and immediately began filming cells at 37 °C. Again, we found that BCCIP-deficient cells took longer time than the control to complete mitosis after recovery from disassembly of the spindle (Figure 9e). Therefore, the mitotic delay experienced by BCCIP-deficient cells is dependent on proper spindle assembly.

DISCUSSION

In this study we identify BCCIP, especially BCCIPα, as a novel MAP that localizes to the interphase centrosome and the mitotic spindle poles. We conclude that BCCIP is critical for microtubule organizing and anchoring activities during interphase, and this function is later co-opted to organize and stabilize the spindle pole during mitosis. In the absence of BCCIP, the interphasic microtubule network fails to maintain its normal association with the centrosome, leading to a general disorganization and destabilization of microtubule arrays, concomitant with an increase of morphologically abnormal cells and decreased acetyl-tubulin. This observation is consistent with BCCIP's association with p150 glued/dynactin and localization to the mother centriole. During mitosis, the microtubule-binding abilities of BCCIP are directed by the minus-end motor dynein to coordinate the micro-tubule's minus end with the centrosome in order to generate spindle tension. These observations are consistent with the collapsed, defocused spindles observed during BCCIP silencing, which display decreased bivalent distance and are sequestered in mitosis. It is important to note that these defects are a phenocopy silencing of the dynein/dynactin/NuMa epistasis group. The totality of this evidence coupled with the physical association of BCCIP with dynactin suggests that these proteins lie within the same pathway.

The coordinated activity of molecular motors with minus-end MAPs is required to focus microtubule minus ends.[1] Silencing of dynein, dynactin, as well as spindle pole MAPs, such as NuMA, results in spindle splaying, lagging chromosomes and delayed mitotic progression in cultured cells.[16,37] Genetic deletion of these factors in vertebrates results in embryonic lethality and/or aneuploidy, suggesting that this network is essential for both the rapid cell divisions that characterize embryonic development and for the maintenance of genome integrity.[13,15,38] We suggest that the microtubule organizing function of BCCIP acts as a safeguard against tumorigenesis and its loss is another root cause of the excessive level of aneuploidy observed in BCCIP-deficient cells by previous works.[25,26]

During development, cell division is critical for regulating not only cell number but also cell diversity.[53] Although symmetric cell division facilitates rapid clonal expansion, asymmetric division is responsible for cell lineage diversification.[53] For example, verte-brate neurogenesis is heralded by a sequence of symmetric and asymmetric cell divisions exquisitely orchestrated to generate the remarkable cellular diversity and complex tissue architecture of the brain.[53,54] Consequently, defects in genes that regulate the orientation of the mitotic spindle and the fidelity of the centrosome are endemic to human brain diseases.[9,53–55] Among the most prominent is primary microcephaly, a condition that results in an abnormally small brain and other neurological disorders. Remarkably, all identified microcephaly genes are centrosome and mitotic spindle regulators, and their knockdown in both cultured cells and in mice induces abnormal organization of interphase microtubule arrays and mitotic defects.[53,56,57] We have previously observed that BCCIP knockdown leads to microcephaly and altered cell differentiation in the neural cortex in mice[58] and therefore the propose that the microcephaly experienced in BCCIP-deficient mice may be related in part to defective asymmetric division.

It is interesting to note that of two BCCIP isoforms, BCCIPα is the predominant centrosome and microtubule-associated isoform. Despite this observation, the recruitment of BCCIPα to spindle poles is dependent on amino acids 111–257, a region shared by both BCCIPα and BCCIPβ. It is of note that this domain predicts a highly conserved coiled coil, a major structural motif responsible for pericentriolar matrix anchoring.[59] We demonstrate that BCCIPα is the predominant isoform that associates with the spindle and centrosome in vivo, yet the C-terminal domains that diversify BCCIPα from BCCIPβ have little role in spindle targeting. This is consistent with the observation that in mouse cells where BCCIPα is not available, the BCCIPβ-like isoform of BCCIP localizes to the centrosome and spindle poles in an identical manner to human BCCIPα. Despite this observation, in nearly all of our biochemical experiments, we were able to detect an association of human BCCIPβ with spindle components following cell lysis, which supports the notion that the inhibition of targeting of BCCIPβ to the centrosome may only be relevant in vivo, and is possibly influenced by transacting elements that are lost after the cell lysis during biochemical manipulation.

In summary, our study has established BCCIP as a previously unidentified regulator of spindle assembly that cooperates with the dynein epistatic group to ensure the fidelity of mitosis. Our data not only describe a new functional aspect of the BCCIP gene but also expand the list of factors critical for mitotic progression, spindle orientation and microtubule organizing.

MATERIALS AND METHODS

Microscopes

Confocal microscopy image capture and analysis was performed on a Nikon A1 and the Nikon elements software suite. Otherwise, for standard epifluorescence, a Nikon eclipse TS100 microscope was used in conjunction with Image-J. Live microscopy was performed on a Zeiss Axiovert 200M and analysis was achieved using the Axiovision software.

Cell culture, expression of transgenes and drug treatment

All cell culture reagents were purchased from Sigma-Aldrich (St. Louis, MO, USA), except stated specifically. HT1080, Cos-7, 293 T, U2OS and HeLa cells were cultured in α-Dulbecco's Modified Eagle's Medium, with 10% fetal bovine serum, 20 mm glutamine and 1% penicillin–streptomycin. Mouse embryonic fibroblasts were isolated as described previously[25] and routinely maintained in the same media as above. For transgene expression, cells were seeded overnight and were transfected at 80% confluence (100 mm dish) with 10 µg plasmid DNA using the RU-50 transfection reagent (Syd-Labs, MB088-450-20, MA, USA) according to the manufacturer's instructions. Twenty-four hours after transfection, the media was aspirated, and cells were processed for specific assays such as immunofluorescence staining or western blotting. To establish cells with stable transgene expression including YFP/Flag-BCCIP or GFP-tubulin, the transfected cells were subjected to antibiotic selection including puromycin (Sigma 2 µg/ml) or G418 (400 µg/ml) depending on the vector, starting at 48 h after transfection. Positive single clones were obtained, and the population was expanded to provide stable cell lines.

Plasmid vectors and production of retrovirus and lentivirus

The pLXSN vector (Clontech, Mountain View, CA, USA 631509) and its derivative pLXSP[30] was utilized for retroviral packaging. A panel of YFP-BCCIP fragments from a BCCIP cDNA as EcoRI/BamHI fragments were cloned into the pLXSN-YFP retroviral backbone. In order to mutate wild-type BCCIPα in the pLXSN-BCCIP vector, BCCIP deletion fragments were created using a PCR splicing strategy.[60] The YFP deletion constructs were also inserted as an EcoRI/NotI fragment into the pCMV-Myc vector (Clontech, 631604) for transient expression. The procedure to package retrovirus has been previously described.[30] The backbone of the H1P-HygroEGFP lentivirus vector[61] was modified by replacing the HygroEFGP sequence with that of GFP or Puromycin marker, resulting in H1P-shRNA-GFP or H1P-shRNA-Pur vectors. The following pairs of oligonucleotides were synthesized: 5'GGCCTTCTCCTAAGTGAAATTCAAGAGATTTCACTTA GGAGAAGGCCTTTTTTG3' and its reverse complement of 5'CAAAAAA GGCCTTCTCCTAAGTGAAATCTCTTGAATTTCACTTAGGAGAAGGCC3'. A total of 5 mm of each oligo was mixed, heated at 95 °C and allowed to cool to anneal complementary oligos. The resulting double-stranded nucleotide was cloned into the vectors through the XbaI and EcoRI sites, resulting in H1P-shBCCIP552-GFP and H1P-shBCCIP552-Pur. In this construct, the BCCIP shRNA expression is under the control of the hH1P promoter, and the expressed shRNA targets the common region of 5'GGCCUUCU CCUAAGUGAAAGA3' starting at location 552nt in the BCCIPα and BCCIPβ RNAs. To generate lentivirus particles, the 293 T cells were seeded at 70% confluence. The next day, cells were cotransfected with 6 µg H1P-shBCCIP552-GFP or H1P-shBCCIP552-Pur, 3 µg psPAX2 (Addgene, Cambridge, MA, USA #12260) and 3 µg pMD2G (Addgene #12259). At 48 h post transfection, virus-containing supernatant was collected, filtered through a 0.45 µm nylon mesh and adjusted to 8 µg/ml polybrene (Sigma 107689). Target cells (HeLa, HT1080, and U2OS) were incubated with viral supernatant overnight. Eighteen hours later, the supernatant was aspirated and the cells were allowed to recover overnight. Infection efficiency was evaluated by observing GFP expression 72 h after the initial infection. Alternatively, stable shBCCIP expressing cells were selected in puromyicin (Sigma 2 µg/ml) for 48 h when the H1P-shBCCIP552-Pur vector was used. The H1P-shRNA-GFP or H1P-shRNA-Pur vector backbone was used as negative control. Knockdown cells were discarded following three passages.

Antibodies and western blots

The rabbit anti-BCCIP BR5 and S1472-2 antibodies were custom-made using recombinant BCCIP protein as the antigens. The commercial antibodies purchased for fluorescent immunostaining and western blot include the following: α-tubulin (Sigma DM1A, 1:500), γ-tubulin (Sigma GTU-88, 1:1000), K-40 Acetyl α-tubulin (Sigma 6-11B-1, 1:500), Phospho H3-T11 (Cell Signaling Technology, Danvers, MA, USA #9764 1:500), Plk-1 (Santa Cruz Monoclonal F-8 1:100), GAPDH (Cell Signaling Technology #14C10, 1:100, or Santa Cruz Biotechnology, Inc., Dallas, TX, USA 6C5 1:2000), Pericentrin (Covance, Denver, PA, USA PRB-432C, 1:300), CREST (Immunovision, Springdale, AR, USA HCT0100, 1:1000), CENP-E (Santa Cruz Biotechnology, Inc. H-300, 1:500), GST (Santa Cruz Biotechnology, Inc. B-14 1:500), CoxIV (Cell Signaling Technology 3E11, 1:100), Lamin A/C (Cell Signaling Technology 4C11 1:1000), PCNA (Invitrogen, Carlsbad, CA, USA PC-10 1:1000), GFP (Santa Cruz Biotechnology, Inc. sc-8334 1:1000), Aurora-A (Cell Signaling Technology 1G4 1:500), HSP90 (Cell Signaling Technology C45G5 1:1000), CDC2 (Invitrogen A17 1:1000), and Flag (Cell Signaling Technology 1:500 #2368) Cyclin B (Santa Cruz Biotechnology, Inc. GNS1 1:200) p150 (BD Labs, Franklin Lakes, NJ, USA 1:100 #610473) Arp1 (1:300 Sigma A5601).

To perform western blots, cells were lysed in RIPA buffer (50 mm Tris HCl, pH 7.4, with 150 mm NaCl, 1 mm EDTA, and 1% Triton X-100, 0.1% SDS, 0.1% sodium deoxycholate 1 mm Leupeptin, 1 mm Aprotinin, 20 mm PMSF). Lysates were subjected to electrophoresis and transferred to nitrocellulose. The membranes were blocked in 1% milk for 1 h, and incubated overnight with the specified antibodies. Following incubation, membranes were washed four times in 0.1% Tween-20-TBST, and incubated for 1 h with HRP anti-mouse or anti-rabbit IgG secondary antibodies (Sigma 1:2500). Membranes were then washed as above and proteins were detected using ECL (Promega, Fitchburg, WI, USA).

Immunofluorescence staining

To perform immunofluorescent staining, cells were seeded onto poly-L-lysine-treated coverslips in a six-well plate at 60% confluence. Forty-eight hours after seeding, the medium was aspirated and cells were extracted at 37 °C D-BRB80 buffer (50 µg/ml M8A, B and M9A, D.igitonin, 80 mm PIPES (pH 6.9), 30% glycerol, 1 mm EGTA, 1 mm MgCl2) or 37°C T-BRB80 (0.3% Triton X-100, 80 mm PIPES (pH 6.9), 30% glycerol, 1 mm EGTA, 1 mm MgCl2) for 1 min. The extraction buffer was aspirated and cells were then fixed at 37 °C in 4% paraformaldehyde for 20 min. Following fixation, the slides were blocked in 0.3% Triton, 5% bovine serum albumin for 1 h (immunofluorescent block buffer). Cells were immunostained overnight in blocking buffer with the indicated antibodies. The slides were then washed thrice in PBS+0.1% Triton X-100 for 5 min. Slides were incubated with 1:1000 dilution of FITC or TRITC anti-mouse, anti-rabbit or anti-human conjugated secondary antibodies (1:1000, Sigma) for 1 h in blocking buffer. The slides were washed as above, and mounted onto coverslips with Vectashield mounting media containing 4',6-diamidino-2-phenylindole (DAPI).

Exogenous expression of RNAi-resistant BCCIP

Because the shRNA expressed from the lentivirus was designed to target the BCCIP mRNA at the following site: GGGCCUUCUCCUAAGUGAA-AGA, transgenic RNAi-resistant constructs were created by mutating four nucleotides in the shRNA-targeted region of BCCIP cDNA to 5'-GGGCTTCTGCTCAGCGAAAGA-3'. This produces silent point mutations in the BCCIP cDNAs (designated BCCIPα^{M4}, and BCCIPβ^{M4}), which codes for exogenous BCCIP that is resistant to shRNA targeted at the same site of the endogenous BCCIP. In this study, we express these shBCCIP552-resistant BCCIPα^{M4} and BCCIPβ^{M4} variants in BCCIP knockdown cells in order to test which BCCIP isoform can rescue the defects caused by BCCIP knockdown and to rule out off-target effect.

Measurement of centriole bias

In order to determine marker colocalization, GFP-EB1 expressing cells were costained with BCCIP and γ-tubulin. Centriole bias was calculated by obtaining 0.2-micron centrosome stacks in T-BRB80 paraformaldehyde fixed cells that exhibited two clearly separate γ-tubulin puncta. Image-J was then utilized to measure the fluorescent intensity of each marker in individual γ-tubulin foci, and the fluorescent intensity of each marker was divided by one another to obtain a ratio. γ-tubulin was utilized as a reference (no bias; ratio of 1), while EB1 was utilized as a mother centriole marker as previously reported.[17,39,40]

Quantitative comparison of immunofluorescent intensity between two cell types

In order to reliably and quantitatively compare the intensity of fluorescent signals between cells of two different genotypes, we co-seeded cells of two different genotypes at a 1:1 ratio, and proceeded with immuno-fluorescent staining. For example, in order to quantitatively compare acetyl-tubulin intensity between BCCIP knockdown and knockdown cells complemented with exogenous YFP-BCCIPα, YFP-BCCIPα expressing cells (green cells) were mixed with BCCIP knockdown cells (no color). The mixed cells were grown to 80% confluency, extracted with T-BRB80 and fixed in fresh paraformaldehyde. Microscope fields containing both YFP-expressing (complemented) and YFP-negative cells were imaged for acetyl-tubulin intensity, using the ×60 objective of a Nikon eclipse TS100 microscope.

4764

Only images containing both cell types (as confirmed by BCCIP staining or GFP markers) were scored. This procedure uses stringent internal control within the same individual slides and allows us to eliminate any potential discrepancy that may be associated with variation of staining and image acquisition procedures. On each image, the polygon tool in Image-J was utilized to measure the fluorescent intensity in the cells containing high levels of BCCIP to cells where BCCIP staining was not visible. Fluorescent intensity was calculated using the following formula (Fluorescent intensity = Integrated Density − (Area of selected × Mean fluorescence of background readings). Intensities of > 100 cells were quantified for each cell type, the fluorescent intensity of all slides was pooled, and subjected to Student's t-test to determine the statistical significance. In some cases, Nikon-elements AR software suite was utilized to calculate the fluorescent density from the regions of interest of an image.

Protein interaction assays: GST-fusion protein pull down

Because the locations of endogenous α-, β- and γ-tubulins overlap with that of the 50 kD IgG used in a routine immunoprecipitation experiment and this precludes the accurate detection of the amount of tubulin coprecipitated by BCCIP, we used GST-BCCIP fusion proteins to coprecipitate endogenous tubulin. GST-BCCIP proteins were incubated with 1 mg spindle fraction prepared from mitotic cell lysates as described elsewhere.[62] We added 50 µl glutathione resin (Novagen, Madison, WI, USA) to this mixture and incubated overnight. The beads were spun down and washed five times in PBS 0.1% Triton, and eluted three times in 10 mM reduced glutathione. To test the direct binding between BCCIP and tubulin, 10 µg GST-tagged BCCIPα, BCCIPβ or GST were incubated with 5 µg of purified bovine tubulin (cytoskeleton) in T-BRB80 without glycerol. The eluted GST-BCCIP bound proteins along with the input were then subjected to SDS-PAGE and western blotting.

Isolation of mitotic centrosomes

The mitotic centrosomes were isolated using a procedure described previously, with some modifications.[33,63] Briefly, HeLa cells were grown in 10 150 mm dishes until 80% confluence and were arrested in 5 mM thymidine overnight. The thymidine containing media was aspirated, cells were washed three times in PBS, and cells were incubated overnight in fresh media containing 100 ng/ml nocodazole (Sigma). The next day the media was adjusted to 5 µg/ml nocodazole, 1 µg/ml Cytochalasin-D (Sigma) and cells were incubated an additional hour. Cells were typsinized and resuspended in ice-cold media, pelleted, and washed sequentially in ice cold PBS, ice-cold PBS diluted tenfold in water, and ice-cold water in 8% sucrose. Following the last wash, cells were lysed in centrosome lysis buffer (0.5% Triton X-100, 1 mM Tris pH 7.0). The remaining procedure was performed identically to procedures outlined elsewhere.[33,63] For immunofluorescence, the peak centrosome fraction was collected, diluted in 5 ml 10 mM PIPES and centrifuged at 10 000 × G (SW-41 Rotor) through a 30% glycerol onto a coverslip. The coverslip was carefully removed, fixed in 100% methanol, and processed with the immunofluorescence procedure described above.

Differential extraction of centrosome proteins

To evaluate the association strength of centrosome proteins, the same assay as reported was used.[35] Briefly, centrosome fractions were pooled, diluted in 5 ml 10 mM PIPES and divided into four microcentrifuge tubes. Centrosomes were pelleted at 20 000 × g and the supernatant was aspirated. Pellets were incubated with 1D Buffer (0.5% Triton X-100), 2D Buffer (0.5% Triton X-100 and 0.5% deoxycholate), 3D buffer (0.5% Triton X-100, 0.1% SDS and 0.5% deoxycholate) or 8 M urea. Pellet and supernatant fractions were separated by centrifugation at 20 000 × g, the supernatant was collected and the pellet was solubilized in boiling Laemmli buffer (30 mM Tris-HCl, pH 6.8, 1% SDS, 10% (w/v) glycerol, 0.01% bromophenol blue, 10% β-mercaptoethanol). Equal portions of pellet and supernatant were utilized for western blotting.

Microtubule spin down assay

To measure the interaction of BCCIP with mitotic microtubules, we modified the procedure described by Young et al.[36] Briefly, HeLa or Cos-7 cells expressing BCCIP or BCCIP fragments were grown to 80% confluency in 150 mm dishes, blocked with 5 mM thymidine overnight, washed, and released into fresh media containing 100 ng/ml nocodazole. Eighteen hours later, cells were harvested by trypsinization, the nocodazole was removed and cells were lysed and sonicated in tubulin lysis buffer (50 mM Tris HCl, pH 7.4, with 75 mM NaCl, 80 mM PIPES, 1 mM MgCl2 and 0.3% Triton X-100, 1 mM Leupeptin, 1 mM Aprotinin, 20 mM PMSF). The lysate was then cleared by centrifugation for 20 min at 16000 × g. The supernatant was then collected, adjusted with 20 units of benzonase (Sigma) and the lysate was precleared again by centrifugation at 100 000 × g in an SW41 rotor for 1 h. The clarified, high-speed lysate (containing the non-polymerized tubulin) was adjusted to 100 mM DTT, 1 mM EGTA, 100 µg/ml bovine tubulin (cytoskeleton), 1 mM GTP, 50 µM taxol (Sigma) or the same buffer containing 10 µg/ml nocodazole without taxol and centrifuged for 30 min at 50 000 × g in an SW41 rotor over a 30% sucrose cushion containing taxol or nocodazole. The supernatant was collected, the pellet was washed once in tubulin lysis buffer containing taxol or nocodazole, and resuspended in boiling Laemmli buffer. The pellet represents the mitotic microtubule fraction and associated proteins. Equal portion of supernatant and pellet fractions were analyzed by western blotting.

Microtubule regrowth assay and quantification of focused microtubules

A previously reported assay performed was utilized to determine the kinetics of minus-end microtubule assembly.[39,64] GFP-tagged BCCIP knockdown cells were mixed 50/50 with cells transduced with an empty shRNA cassette and seeded onto coverslips. Cells were treated with 5 µg/ml nocodazole, ice-chilled for 1 h and fixed at either 2, 5, 10 and 20 min following nocodazole washout with prewarmed media. Centrosome aster intensity was measured by using the α-tubulin signal around a predefined area from each centrosome with the Image-J circle tool. Only images containing knockdown cells adjacent to control cells (as assessed by GFP) were scored.

Analysis of spindle poles and mitotic spindles

In order to quantify the spindle defects in an unbiased manner, we selected only metaphase cells in which a clear chromosome congression was detected at the metaphase plate. This was accomplished by a 3-h MG-132 block. The pole-to-pole distance was assessed by utilizing Image-J to measure the pole-to-pole distance between pericentrin foci. To measure spindle arc, the angle tool was utilized in Image-J. The second point of the angle tool was consistently placed on the central pericentrin focus and the first and second points were placed 3 microns in length parallel to the α-tubulin-stained mitotic spindle. For the analysis of pole splaying, we measured the length of pericentrin foci at the poles in the control and BCCIP knockdown condition. For quantification of spindle pole components, the polygon tool in Image-J was utilized to trace and measure the intensity of indicated markers at the poles.

Measurement of spindle tilt and off-center spindles

We utilized the method described by Hori et al, including synchronization of metaphase cells.[14] Briefly, cells were plated on collagen-treated coverslips and fixed in 100% methanol, stained with pericentrin, and a series of 0.2-micron stacks were obtained. The signal maxima and the central maxima of pericentrin foci was utilized to measure the horizontal (X) and vertical (Z) distance between the poles, respectively, and spindle tilt was calculated as a function of $\theta = \sin^{-1}(Z/X)$. In order to measure the deviation of the mitotic spindle from the centroid of the cell, we measured the distance of the spindle pole to the closest cortex and acquired a ratio between these values. The higher ratio between cortex distances was consistently used to plot position.

Measurement of distance between kinetochore sister bivalents and chromosome congression

In order to measure metaphase chromosome congression cells were treated by MG-132 for 3 h. Image processing and analysis followed that of Green and Kaplan.[44]

The assay developed by Waters et al.,[49,50] was used to measure the distance between unambiguous sister kinetochore pairs identified CREST staining. Images were collected in a single focal plane for BCCIP control and BCCIP knockdown cells, and the distance between kinetochore bivalents was measured using Image-J.

Measurement of mitotic time, bipolarity, spindle orientation and nocodazole recovery using time-lapse imaging of live cells

HT1080 or U2OS cells stably expressing GFP-tubulin were transduced with H1P-shBCCIP522-Pur lentiviral particles or control lentivirus. Cells were transferred to an incubated microscope (Zeiss Axiovert 200M) and filmed every 5 min using the ×20 objective overnight. The duration of mitosis was quantified by the disappearance of the nuclear envelope to the presence of a visible mid-body. In some experiments, cells were challenged by 1 mg/ml nocodazole overnight, chilled on ice for 1 h the next day, and mitotic cells were filmed following three washes in prewarmed media. Spindle bipolarity onset was quantified by measuring the amount of time cells took to assemble a well-defined metaphase spindle.

Statistics analysis

Data value of individual cells, the average and standard deviations are plotted. Two-tailed and unpaired Student's *t*-test was used to determine the statistical significance between two different cell populations.

CONFLICT OF INTEREST

The authors declare no conflict of interest.

REFERENCES

1 Merdes A, Cleveland DW. Pathways of spindle pole formation: different mechanisms; conserved components. *J Cell Biol* 1997; **138**: 953–956.

2 Hernandez P, Tirnauer JS. Tumor suppressor interactions with microtubules: keeping cell polarity and cell division on track. *Dis Model Mech* 2010; **3**: 304–315.

3 Pellman D. Cell biology: aneuploidy and cancer. *Nature* 2007; **446**: 38–39.

4 Chandhok NS, Pellman D. A little CIN may cost a lot: revisiting aneuploidy and cancer. *Curr Opin Genet Dev* 2009; **19**: 74–81.

5 Namba M, Mihara K, Fushimi K. Immortalization of human cells and its mechanisms. *Crit Rev Oncog* 1996; **7**: 19–31.

6 Ried T, Hu Y, Difilippantonio MJ, Ghadimi BM, Grade M, Camps J. The consequences of chromosomal aneuploidy on the transcriptome of cancer cells. *Biochim Biophys Acta* 2012; **1819**: 784–793.

7 Cimini D, Degrassi F. Aneuploidy: a matter of bad connections. *Trends Cell Biol* 2005; **15**: 442–451.

8 Yang Y, Liu M, Li D, Ran J, Gao J, Suo S *et al*. CYLD regulates spindle orientation by stabilizing astral microtubules and promoting dishevelled-NuMA-dynein/dynactin complex formation. *Proc Natl Acad Sci USA* 2014; **111**: 2158–2163.

9 Godin JD, Colombo K, Molina-Calavita M, Keryer G, Zala D, Charrin BC *et al*. Huntingtin is required for mitotic spindle orientation and mammalian neurogenesis. *Neuron* 2010; **67**: 392–406.

10 Thoma CR, Toso A, Gutbrodt KL, Reggi SP, Frew IJ, Schraml P *et al*. VHL loss causes spindle misorientation and chromosome instability. *Nat Cell Biol* 2009; **11**: 994–1001.

11 Bornens M. Centrosome composition and microtubule anchoring mechanisms. *Curr Opin Cell Biol* 2002; **14**: 25–34.

12 Nigg EA, Stearns T. The centrosome cycle: Centriole biogenesis, duplication and inherent asymmetries. *Nat Cell Biol* 2011; **13**: 1154–1160.

13 Fukasawa K. Oncogenes and tumour suppressors take on centrosomes. *Nat Rev Cancer* 2007; **7**: 911–924.

14 Hori A, Ikebe C, Tada M, Toda T. Msd1/SSX2IP-dependent microtubule anchorage ensures spindle orientation and primary cilia formation. *EMBO Rep* 2014; **15**: 175–184.

15 Khodjakov A, Cole RW, Oakley BR, Rieder CL. Centrosome-independent mitotic spindle formation in vertebrates. *Curr Biol* 2000; **10**: 59–67.

16 Haren L, Gnadt N, Wright M, Merdes A. NuMA is required for proper spindle assembly and chromosome alignment in prometaphase. *BMC Res Notes* 2009; **2**: 64.

17 Louie RK, Bahmanyar S, Siemers KA, Votin V, Chang P, Stearns T *et al*. Adenomatous polyposis coli and EB1 localize in close proximity of the mother centriole and EB1 is a functional component of centrosomes. *J Cell Sci* 2004; **117**(Pt 7): 1117–1128.

18 Quintyne NJ, Schroer TA. Distinct cell cycle-dependent roles for dynactin and dynein at centrosomes. *J Cell Biol* 2002; **159**: 245–254.

19 Guo J, Yang Z, Song W, Chen Q, Wang F, Zhang Q *et al*. Nudel contributes to microtubule anchoring at the mother centriole and is involved in both dynein-dependent and -independent centrosomal protein assembly. *Mol Biol Cell* 2006; **17**: 680–689.

20 Kim DJ, Martinez-Lemus LA, Davis GE. EB1, p150Glued, and Clasp1 control endothelial tubulogenesis through microtubule assembly, acetylation, and apical polarization. *Blood* 2013; **121**: 3521–3530.

21 Kline-Smith SL, Walczak CE. Mitotic spindle assembly and chromosome segregation: refocusing on microtubule dynamics. *Mol Cell* 2004; **15**: 317–327.

22 Audhya A, Emr SD. Regulation of PI4,5P2 synthesis by nuclear-cytoplasmic shuttling of the Mss4 lipid kinase. *EMBO J* 2003; **22**: 4223–4236.

23 Fan J, Wray J, Meng X, Shen Z. BCCIP is required for the nuclear localization of the p21 protein. *Cell Cycle* 2009; **8**: 3019–3024.

24 Lu H, Guo X, Meng X, Liu J, Allen C, Wray J *et al*. The BRCA2-interacting protein BCCIP functions in RAD51 and BRCA2 focus formation and homologous recombinational repair. *Mol Cell Biol* 2005; **25**: 1949–1957.

25 Lu H, Huang YY, Mehrotra S, Droz-Rosario R, Liu J, Bhaumik M *et al*. Essential roles of BCCIP in mouse embryonic development and structural stability of chromosomes. *PLoS Genet* 2011; **7**: e1002291.

26 Lu H, Yue J, Meng X, Nickoloff JA, Shen Z. BCCIP regulates homologous recombination by distinct domains and suppresses spontaneous DNA damage. *Nucleic Acids Res* 2007; **35**: 7160–7170.

27 Mao N, Zhou Q, Kojic M, Perez-Martin J, Holloman WK. Ortholog of BRCA2-interacting protein BCCIP controls morphogenetic responses during DNA replication stress in *Ustilago maydis*. *DNA Repair* 2007; **6**: 1651–1660.

28 Meng X, Yue J, Liu Z, Shen Z. Abrogation of the transactivation activity of p53 by BCCIP down-regulation. *J Biol Chem* 2007; **282**: 1570–1576.

29 Huang YY, Dai L, Gaines D, Droz-Rosario R, Lu H, Liu J *et al*. BCCIP suppresses tumor initiation but is required for tumor progression. *Cancer Res* 2013; **73**: 7122–7133.

30 Liu J, Yuan Y, Huan J, Shen Z. Inhibition of breast and brain cancer cell growth by BCCIPalpha, an evolutionarily conserved nuclear protein that interacts with BRCA2. *Oncogene* 2001; **20**: 336–345.

31 Wyler E, Wandrey F, Badertscher L, Montellese C, Alper D, Kutay U. The beta-isoform of the BRCA2 and CDKN1A(p21)-interacting protein (BCCIP) stabilizes nuclear RPL23/uL14. *FEBS Lett* 2014; **588**: 3685–3691.

32 Meng X, Liu J, Shen Z. Genomic structure of the human BCCIP gene and its expression in cancer. *Gene* 2003; **302**: 139–146.

33 Hsu LC, White RL. BRCA1 is associated with the centrosome during mitosis. *Proc Natl Acad Sci USA* 1998; **95**: 12983–12988.

34 Wang HF, Takenaka K, Nakanishi A, Miki Y. BRCA2 and nucleophosmin coregulate centrosome amplification and form a complex with the Rho effector kinase ROCK2. *Cancer Res* 2011; **71**: 68–77.

35 Keryer G, Di Fiore B, Celati C, Lechtreck KF, Mogensen M, Delouvee A *et al*. Part of Ran is associated with AKAP450 at the centrosome: involvement in microtubule-organizing activity. *Mol Biol Cell* 2003; **14**: 4260–4271.

36 Young A, Dictenberg JB, Purohit A, Tuft R, Doxsey SJ. Cytoplasmic dynein-mediated assembly of pericentrin and gamma tubulin onto centrosomes. *Mol Biol Cell* 2000; **11**: 2047–2056.

37 Raaijmakers JA, Tanenbaum ME, Medema RH. Systematic dissection of dynein regulators in mitosis. *J Cell Biol* 2013; **201**: 201–215.

38 Howell B, McEwen B, Canman J, Hoffman D, Farrar E, Rieder C *et al*. Cytoplasmic dynein/dynactin drives kinetochore protein transport to the spindle poles and has a role in mitotic spindle checkpoint inactivation. *J Cell Biol* 2001; **155**: 1159–1172.

39 Delgehyr N, Sillibourne J, Bornens M. Microtubule nucleation and anchoring at the centrosome are independent processes linked by ninein function. *J Cell Sci* 2005; **118**(Pt 8): 1565–1575.

40 Mogensen MM, Malik A, Piel M, Bouckson-Castaing V, Bornens M. Microtubule minus-end anchorage at centrosomal and non-centrosomal sites: the role of ninein. *J Cell Sci* 2000; **113**(Pt 17): 3013–3023.

41 Song Y, Brady ST. Post-translational modifications of tubulin: pathways to functional diversity of microtubules. *Trends Cell Biol* 2015; **25**: 125–136.

42 Shida T, Cueva JG, Xu Z, Goodman MB, Nachury MV. The major alpha-tubulin K40 acetyltransferase alphaTAT1 promotes rapid ciliogenesis and efficient mechanosensation. *Proc Natl Acad Sci USA* 2010; **107**: 21517–21522.

43 Vos MD, Martinez A, Elam C, Dallol A, Taylor BJ, Latif F *et al*. A role for the RASSF1A tumor suppressor in the regulation of tubulin polymerization and genomic stability. *Cancer Res* 2004; **64**: 4244–4250.

44 Green RA, Kaplan KB. Chromosome instability in colorectal tumor cells is associated with defects in microtubule plus-end attachments caused by a dominant mutation in APC. *J Cell Biol* 2003; **163**: 949–961.

45 Heald R, Tournebize R, Habermann A, Karsenti E, Hyman A. Spindle assembly in Xenopus egg extracts: respective roles of centrosomes and microtubule self-organization. *J Cell Biol* 1997; **138**: 615–628.

46 Heald R, Tournebize R, Blank T, Sandaltzopoulos R, Becker P, Hyman A et al. Self-organization of microtubules into bipolar spindles around artificial chromosomes in Xenopus egg extracts. *Nature* 1996; **382**: 420–425.

47 King JM, Nicklas RB. Tension on chromosomes increases the number of kinetochore microtubules but only within limits. *J Cell Sci* 2000; **113**(Pt 21): 3815–3823.

48 DeLuca JG, Dong Y, Hergert P, Strauss J, Hickey JM, Salmon ED et al. Hec1 and nuf2 are core components of the kinetochore outer plate essential for organizing microtubule attachment sites. *Mol Biol Cell* 2005; **16**: 519–531.

49 Waters JC, Chen RH, Murray AW, Salmon ED. Localization of Mad2 to kinetochores depends on microtubule attachment, not tension. *J Cell Biol* 1998; **141**: 1181–1191.

50 Waters JC, Skibbens RV, Salmon ED. Oscillating mitotic newt lung cell kinetochores are, on average, under tension and rarely push. *J Cell Sci* 1996; **109**(Pt 12): 2823–2831.

51 Jackman M, Lindon C, Nigg EA, Pines J. Active cyclin B1-Cdk1 first appears on centrosomes in prophase. *Nat Cell Biol* 2003; **5**: 143–148.

52 Lara-Gonzalez P, Westhorpe FG, Taylor SS. The spindle assembly checkpoint. *Curr Biol* 2012; **22**: R966–R980.

53 Thornton GK, Woods CG. Primary microcephaly: do all roads lead to Rome? *Trends Genet* 2009; **25**: 501–510.

54 Basto R, Lau J, Vinogradova T, Gardiol A, Woods CG, Khodjakov A et al. Flies without centrioles. *Cell* 2006; **125**: 1375–1386.

55 Kops GJ, Weaver BA, Cleveland DW. On the road to cancer: aneuploidy and the mitotic checkpoint. *Nat Rev Cancer* 2005; **5**: 773–785.

56 Gruber R, Zhou Z, Sukchev M, Joerss T, Frappart PO, Wang ZQ. MCPH1 regulates the neuroprogenitor division mode by coupling the centrosomal cycle with mitotic entry through the Chk1-Cdc25 pathway. *Nat Cell Biol* 2011; **13**: 1325–1334.

57 Zhou ZW, Tapias A, Bruhn C, Gruber R, Sukchev M, Wang ZQ. DNA damage response in microcephaly development of MCPH1 mouse model. *DNA Repair* 2013; **12**: 645–655.

58 Huang YY, Lu H, Liu S, Droz-Rosario R, Shen Z. Requirement of mouse BCCIP for neural development and progenitor proliferation. *PLoS One* 2012; **7**: e30638.

59 Salisbury JL. Centrosomes: coiled-coils organize the cell center. *Curr Biol* 2003; **13**: R88–R90.

60 Heckman KL, Pease LR. Gene splicing and mutagenesis by PCR-driven overlap extension. *Nat Protoc* 2007; **2**: 924–932.

61 Ivanova N, Dobrin R, Lu R, Kotenko I, Levorse J, DeCoste C et al. Dissecting self-renewal in stem cells with RNA interference. *Nature* 2006; **442**: 533–538.

62 Skop AR, Liu H, Yates J 3rd, Meyer BJ, Heald R. Dissection of the mammalian midbody proteome reveals conserved cytokinesis mechanisms. *Science* 2004; **305**: 61–66.

63 Mitchison TJ, Kirschner MW. Isolation of mammalian centrosomes. *Methods Enzymol* 1986; **134**: 261–268.

64 Sehrawat S, Ernandez T, Cullere X, Takahashi M, Ono Y, Komarova Y et al. AKAP9 regulation of microtubule dynamics promotes Epac1-induced endothelial barrier properties. *Blood* 2011; **117**: 708–718.

Supplementary Information accompanies this paper on the Oncogene website (http://www.nature.com/onc)